Lithos 286–287 (2017) 454–479

Contents lists available at ScienceDirect

Lithos

journal homepage: www.elsevier.com/locate/lithos

Primary crustal melt compositions: Insights into the controls, mechanisms and timing of generation from kinetics experiments and melt inclusions

Antonio Acosta-Vigil [a,b,*], David London [c], George B. Morgan VI [c], Bernardo Cesare [a], Ian Buick [d], Jörg Hermann [e,f], Omar Bartoli [a]

[a] Dipartimento di Geoscienze, Università degli Studi di Padova, Via Giovanni Gradenigo 6, 35131 Padova, Italy
[b] Instituto Andaluz de Ciencias de la Tierra, Consejo Superior de Investigaciones Científicas and Universidad de Granada, Armilla, Granada, Spain
[c] School of Geology and Geophysics, University of Oklahoma, Norman, OK, USA
[d] Department of Earth Sciences, Stellenbosch University, Stellenbosch, South Africa
[e] Institute of Geological Sciences, University of Bern, Bern, Switzerland
[f] Research School of Earth Sciences, Australian National University, Canberra, Australia

ARTICLE INFO

Article history:
Received 11 February 2016
Accepted 29 May 2017
Available online 3 June 2017

Keywords:
Crustal anatexis
Granite
Mechanisms
Kinetics
Primary melt composition
Nanogranitoids

ABSTRACT

We explore the controls, mechanisms and timing of generation of primary melts and their compositions, and show that the novel studies of melt inclusions in migmatites can provide important insights into the processes of crustal anatexis of a particular rock. Partial melting in the source region of granites is dependent on five main processes: (i) supply of heat; (ii) mineral–melt interface reactions associated with the detachment and supply of mineral components to the melt, (iii) diffusion in the melt, (iv) diffusion in minerals, and (v) recrystallization of minerals. As the kinetics of these several processes vary over several orders of magnitude, it is essential to evaluate in Nature which of these processes control the rate of melting, the composition of melts, and the extent to which residue–melt chemical equilibrium is attained under different circumstances. To shed light on these issues, we combine data from experimental and melt inclusion studies. First, data from an extensive experimental program on the kinetics of melting of crustal protoliths and diffusion in granite melt are used to set up the necessary framework that describes how primary melt compositions are established during crustal anatexis. Then, we use this reference frame and compare compositional trends from experiments with the composition of melt inclusions analyzed in particular migmatites. We show that, for the case of El Hoyazo anatectic enclaves in lavas, the composition of glassy melt inclusions provides important information on the nature and mechanisms of anatexis during the prograde suprasolidus history of these rocks, including melting temperatures and reactions, and extent of melt interconnection, melt homogenization and melt–residue equilibrium. Compositional trends in several of the rehomogenized melt inclusions in garnet from migmatites/granulites in anatectic terranes are consistent with diffusion in melt-controlled melting, though trace element compositions of melt inclusions and coexisting minerals are necessary to provide further clues on the nature of anatexis in these particular rocks.

1. Introduction

Granitic magmas sensu lato play a critical role in both continental crust growth and its internal differentiation. However, the details of processes connecting granitic magmas in their source region with granitic intrusions, or their volcanic equivalents, are far from clear. Focused specifically on the differentiation of continental crust, field-based petrological and geochemical studies of migmatites and allochthonous crustal granites, experimental studies, and phase equilibria modeling, constitute a "3-dimensional" approach to attack this problem (e.g. Brown, 2013; Clemens, 2006; Sawyer, 2008; White et al., 2007, 2011; and references therein). Each of these approaches, however, has drawbacks. Allochthonous granitoids and volcanic equivalents are the end products of anatexis and crustal differentiation, and their study provides a partial view of the process because primary melt compositions are established, and parental magmas generated, at deeper sites of melting. Although exhumed regional migmatitic terranes permit the direct observation of anatectic processes, classical petrological and geochemical studies of these terranes face a number of complexities, which make it difficult to retrieve the primary melt and parental magma compositions. These complexities include that (i) anatectic terranes record the

* Corresponding author at: Research School of Earth Sciences, Australian National University, 142 Mills Road, Acton ACT 0200, Canberra, Australia.
E-mail addresses: acostavigil@hotmail.com, antonio.acostavigil@unipd.it (A. Acosta-Vigil).

http://dx.doi.org/10.1016/j.lithos.2017.05.020

superposition of prograde and retrograde processes, where partial melting occurs concomitantly to differential stress and deformation, (ii) primary melt may have fractionated and partially escaped the system, (iii) perfect segregation of melt from residue seems very unlikely, (iv) melt produced at deeper or adjacent crustal levels may have entered the system, (v) former melt present above the solidus has crystallized upon cooling, and (vi) H_2O dissolved in that melt has escaped and/or reacted with the residue (e.g. Brown, 2002, 2013; Sawyer, 2008, 2014; White and Powell, 2010; and references therein). Most of the experimental studies conducted on crustal anatexis provide equilibrium mineral and melt compositions at particular *P–T–X* conditions, whereas the continental crust is compositionally heterogeneous (Rudnick and Gao, 2003) and, so far, equilibrium melting seems to be the exception rather than the rule (e.g. Bea, 1996; Villaros et al., 2009a). Thermodynamic models also assume melt–solid equilibrium. In addition, there is a lack of precise thermodynamic data for several key phases, or end-members solid solutions related to minor components in the system. This produces, for instance, discrepancies between the compositions of model and natural or experimental melts (e.g. Bartoli et al., 2013a; Grant, 2009; White et al., 2011).

Some studies have concluded that compositional heterogeneities of crustal granitoids are inherited from the source region and, therefore, that somehow they reflect the composition of magmas present at the sites of generation (Clemens and Benn, 2010; Deniel et al., 1987; Glazner et al., 2004; Hogan and Sinha, 1991; Pressley and Brown, 1999). More commonly, however, it is concluded that compositions of crustal granitoids do not correspond to those of the primary anatectic melts produced during their genesis, due to one or a combination of several processes. These include: (i) magmatic differentiation due to e.g. "en route" fractional crystallization, that may start right at or relatively close to the source area (Barr, 1985; Brown et al., 2016; Carvalho et al., 2016; Chappell and White, 1992; Milord et al., 2001; Morfin et al., 2014; Sawyer, 1987, 2014); (ii) entrainment of residual (Chappell, 1996; Chappell et al., 1987), peritectic (Stevens et al., 2007; Villaros et al., 2009b) or both residual and peritectic (García-Arias and Stevens, 2017; Sawyer, 2014) minerals coexisting with the primary melt; (iii) mixing and mingling with mantle derived magmas (Collins, 1996; Gray and Kemp, 2009; Wall et al., 1987). As a consequence of the previous observations, we still have a limited understanding of the nature and intensity of crustal differentiation associated with the geodynamic settings where crustal granitic magmas are produced, including the ratio of crustal growth to crustal reworking (e.g. Brown, 2013).

This contribution seeks to provide information on the very first stages of crustal melting, and particularly on the mechanisms and time frames of melt generation, and controls on the composition of primary melts before segregation from the solid fraction. This represents the starting point of the process of generation of crustal granitoids. Recently, Sawyer (2014) has investigated in a contact metatexite migmatite the earliest stages of segregation of anatectic melts, and concluded that it is accomplished via the movement of melt from in situ neosomes into adjacent 0.5 mm-long micropores and 1 mm-long microleucosomes, that subsequently grow into longer (up to ≈10–20 mm) microleucosomes by progressive destruction of the bridges of matrix separating originally neighboring small microleucosomes. Our study refers to the earliest stages of melting, when melt forms and remains in contact with, or at short diffusion distances from, its residue. During this window of time, several processes leading towards mineral–melt equilibration and melt homogenization may occur, e.g. diffusion in minerals and melt, and recrystallization of minerals. Considering diffusivities of elements in granitic melts at anatectic conditions (e.g. Acosta-Vigil et al., 2012a), together with the shortest reported time frames for melt segregation (Harris et al., 2000; Sawyer, 1991), and estimations of segregation distances associated with the generation of leucosomes (Fig. 1a; Sawyer, 2008, 2014), our study describes the situation possibly before the segregation of melt into microleucosomes and, definitely, before migration of melt into cm–dm-scale in-situ leucosomes. Nevertheless, this time window may vary depending on the tectonic setting and nature of (contact versus regional) anatexis. This contribution, therefore, deals with questions such as what are the controls on the compositions of initial melts generated in different microstructural locations of a protolith, how individual liquid aliquots at different microstructural sites evolve towards a homogeneous melt phase, what are the time frames of melt generation, melt homogenization and melt–residue equilibration, and how these time frames compare with those inferred for separation of melt from residue.

The most direct way to accomplish the investigation of the first stages of melting is through either studies of contact anatectic rocks that reached conditions at, or slightly above their solidus (Holness et al., 2005; Sawyer, 2014), or via experimental simulations (e.g. Acosta-Vigil et al., 2006a; Arzi, 1978; Brearley and Rubie, 1990; Buick et al., 2004; London et al., 2012; Mehnert et al., 1973). Considering the novel studies of melt inclusions (MI) or nanogranitoids in migmatites (Cesare et al., 1997, 2009, 2015), a **brand-new approach** that has the potential to increase our knowledge of the onset of crustal melting and mechanisms of anatexis in particular case studies of migmatites, is the combination of compositional data from MI and experiments on the kinetics of melting. In this contribution, we use previously published but never compared data sets from: (i) experimental studies on the kinetics of melting and diffusion in the granite system (Acosta-Vigil et al., 2012a), and (ii) melt inclusion studies documenting primary melt compositions in (ii.a) anatectic enclaves, where the process of regional partial melting has been frozen due to quenching upon ascent and extrusion within the host magma (Cesare, 2008), and (ii.b) in regional migmatites and granulites (Acosta-Vigil et al., 2016; Bartoli et al., 2016a; Cesare et al., 2015; Ferrero et al., 2015). Thus, we first set up a theoretical scenario describing the several processes acting concomitantly and controlling the nature of primary anatectic melt compositions prior to segregation (Section 2 of the paper); then, we review the results of kinetics experiments providing information on the interplay between, and role/imprint of each of these processes (Section 3); finally, and after discussing the main limitations of experiments to replicate and study natural anatexis (Section 4), we introduce the reader to the study of MI in anatectic rocks, and use the information provided by kinetics experiments as a framework to interpret the previously published compositions of MI in terms of nature and mechanisms of crustal anatexis in Nature (Section 5).

2. Processes and controls during the onset of partial melting: a theoretical scenario

We start by assessing the simplest route to producing a silicate liquid of granitic composition; that is, the melting of a near-minimum granite itself. Consider that a homogeneous, fine-grained crustal rock, such as an aplite, reaches some given *P–T* conditions at or just above its solidus (Fig. 1b). At equilibrium, a certain proportion of homogeneous melt will coexist with an assemblage of homogeneous minerals. However, the equilibrium proportions and compositions of phases will not form instantaneously, and each phase will likely follow a path in proportion (wt%)–composition (*X*)–time (t) space towards the conditions of equilibrium (Fig. 1d). It is the interplay between (i) the kinetics of processes governing the generation and homogenization of melt, and equilibration between melt and residue, versus (ii) the timing of melt segregation and extraction, that will determine the position in wt%–*X*–t space of every single phase at the time of melt–residue separation with respect to their equilibrium values, and hence the extent to which primary anatectic melts are homogeneous and at equilibrium with their bulk residue before leaving the source area.

It is commonly assumed that melting begins at multiphase grain junctions where all necessary reactants meet (e.g. Brown, 2010; Harris et al., 2000; Sawyer, 2014), and that the first melt produced has eutectic composition (e.g. Harris et al., 2000). Although we must be cautious when extrapolating experimental observations to Nature (see

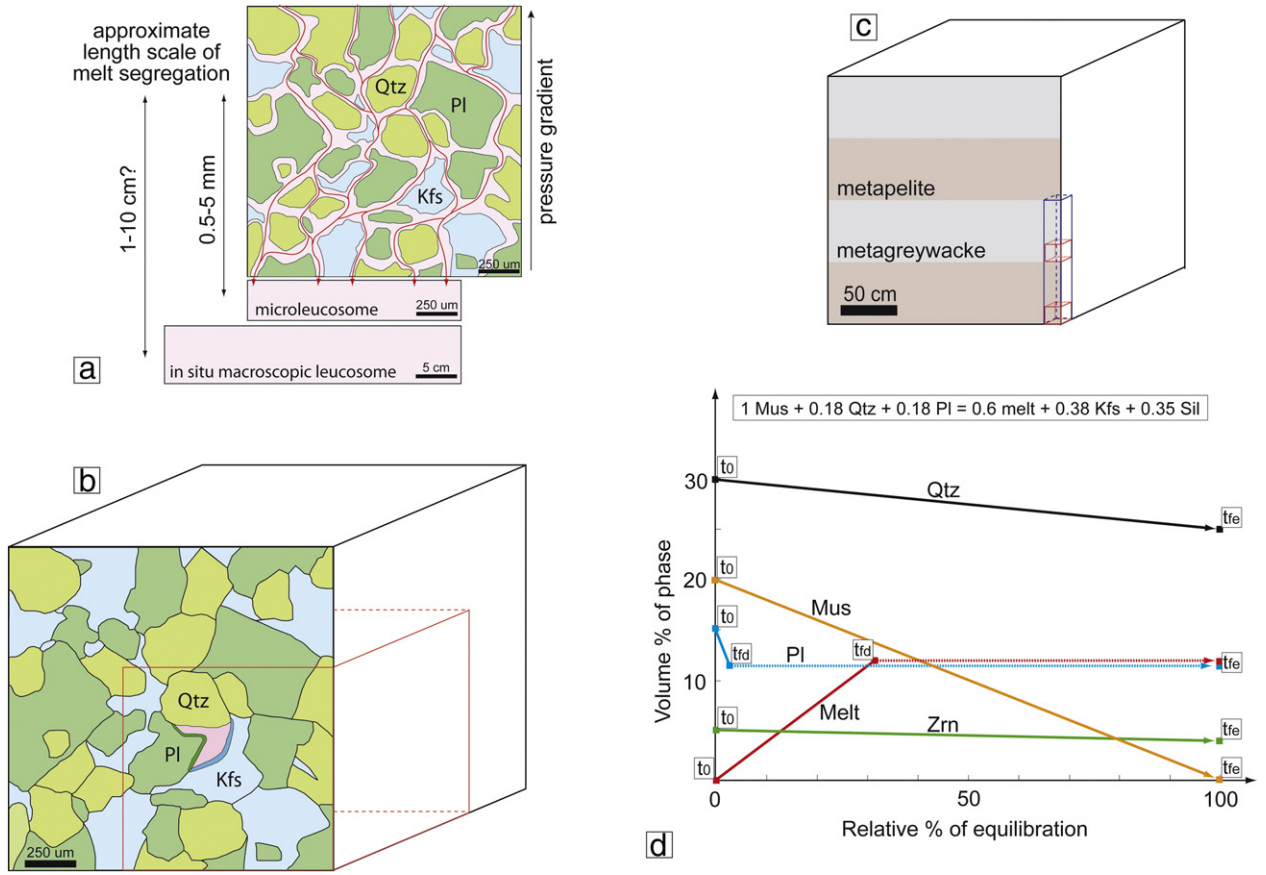

Fig. 1. (a) Schematic representation of a granitic migmatite neosome (melt is shown as the pink interconnected network), showing melt segregation during flow along grain boundaries, due to pressure gradients developed under the effect of differential stress on heterogeneous rocks. Length scales of melt segregation vary from ≈0.5 to 5 mm during generation of microleucosomes, to a few/tens of cm (?) during genesis of in situ macroscopic leucosomes [based on Sawyer (2001) and Sawyer (2008, 2014)]. (b, c) Schematic representations illustrating the concepts of equilibration volume (after Powell and Downes, 1990; Stüwe, 1997) and minimum volume for equilibration during anatexis. (b) Qtz–Pl–Kfs fine-grained homogeneous aplite, showing a Qtz–Pl–Kfs triple junction where partial melting has started, producing a homogeneous melt (pink) at equilibrium with Qtz and locally recrystallized Pl (dark green fringe) and Kfs (dark blue fringe). The equilibration volume corresponds to the melt plus Qtz and recrystallized Pl and Kfs fringes. The minimum volume for equilibrium in this rock corresponds to a cube ≈1–1.5 mm of side length (red cube). Equilibration in this volume guarantees full equilibration in the rock. (c) Compositionally heterogeneous crustal protolith showing banding at the ≈50 cm scale, with the corresponding minimum volume for equilibrium for individual bands (red cubes) and the entire protolith (blue rectangular prism). (d) Schematic diagram showing the evolution (volume % versus relative % of equilibration) of individual phases during the H_2O-absent muscovite-breakdown melting reaction, at the *P*–*T*–*X* conditions of anatexis, and over time (t0, tfd, tfe). In this particular example, the rock mineral composition (in volume %) right before anatexis starts is 30% Qtz + 30% Bt + 20% Ms + 15% Pl + 4% Grt + 1% accessory minerals, the grain size is ≈1 mm, and the length scales of diffusion in melt necessary for chemical equilibration are ≈10 mm (associated with a minimum volume for equilibrium of 125 mm^3, i.e. a cube of 5 mm of length size). The stoichiometry of the melting reaction and proportion of melt generated are taken from Harris et al. (1995) and Clemens and Vielzeuf (1987). "t0" refers to the time when anatexis starts; "tfd" to the time when the reaction has gone to completion regarding volume proportions of phases, but not necessarily in terms of mineral–melt chemical equilibrium due e.g. to the sluggish diffusion of components in minerals; and "tfe" to the time when reaction has gone to completion and mineral–melt chemical equilibrium has been reached. We consider two cases. (1) The rate of melting is controlled by the kinetics of the interface reactions, and there is no recrystallization of minerals. Panel (d) has been drawn for this particular case. In this case, and regarding Qtz, tfe will be > hundreds of years to 1 ky (as in this case rates of interface reaction are slower that rates of diffusion in melt; note that for Qtz, tfd will coincide with tfe); regarding Pl, tfe will be tens of millions of years; and, hence, tfe will be tens of millions of years for the melt as well, as in this case the rate-limiting process controlling chemical equilibrium is diffusion in the minerals (see Sections 2.1, 2.3); mus disappears after reaction has gone to completion. Time frames for Zrn–melt equilibrium regarding Zr concentrations in melt will depend on the distribution in the rock of Zrn crystals accessible to the melt (for Zrn, tfd will also coincide with tfe). (2) The rate of melting is controlled by diffusion in melt, and there is rapid recrystallization of the residual minerals. In this other case, tfe will be of the order of hundreds of years to 1 ky for Qtz, as well as for Pl and melt, as the rate-limiting process controlling chemical equilibrium is diffusion in the melt, and Si is the slowest diffusing component in melt (see Sections 2.2, 2.4, 3.2). In this case tfd will coincide with tfe for all phases.

Section 4), the experimental melting of solid granite cylinders where the distribution and composition of melt through time have been carefully documented, shows that melt forms an interconnected network along most mineral boundaries and cleavages right from the very beginning of melting, e.g. in the shortest 5-day experiment, which is instantaneous at geologic time scales (Fig. 2). In addition, it was found that initial melts are not necessarily eutectic in composition (Acosta-Vigil et al., 2006a). The beginning of crustal melting and establishment of primary melt compositions, therefore, might be more complex than previously considered. Below, we isolate some of the main processes that may occur concomitantly during anatexis.

Theoretically once the first drop of melt has formed at multiphase grain junctions at the very onset of anatexis, there are several processes taking place during static melting, and each of them has its own particular rate; these at least include the following (Fig. 3). (1) Reactions at mineral–melt interfaces which liberate mineral components that enter the melt. (2) Diffusion in the melt of these components in response to chemical gradients, which promotes additional mineral dissolution (if undersaturation persists) and melt homogenization. (3) Diffusion within minerals to equilibrate them with the melt. This includes diffusion of major elements in the case of solid solution minerals, such as Na–Ca in Pl and Fe–Mg in Bt, Grt and Crd (mineral abbreviations after Kretz,

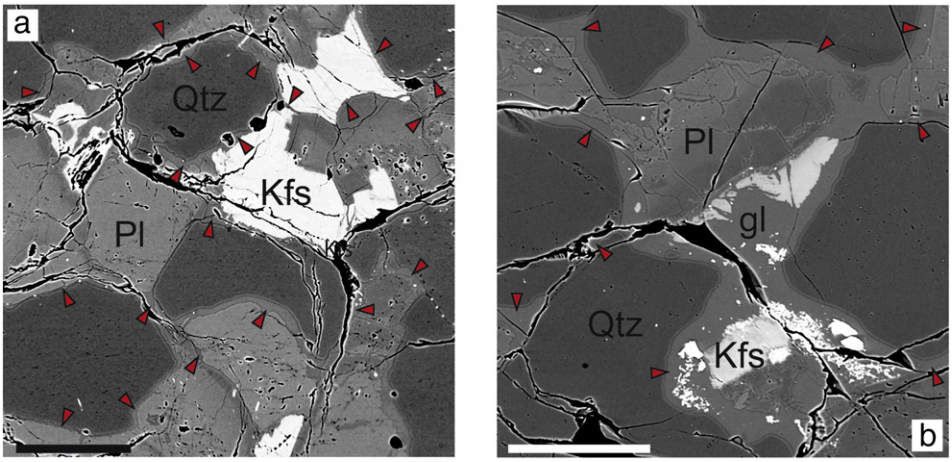

Fig. 2. Backscattered electron (BSE) scanning electron microscope (SEM) images of 690 °C H_2O-saturated melting experiments of aplite at 0.2 GPa, showing the distribution of melt (gl, and shown by red arrow) wetting most of the grain boundaries. (a) 176-h experiment. (b) 744-h experiment. Scale bar is 200 μm in length.
Modified from Fig. 2 of Acosta-Vigil et al. (2006a).

1983); and diffusion of trace elements and isotopes for certain minerals that control their geochemistry during anatexis, such as Sr, Eu in Pl; Ba, Sr, Eu in alkali feldspar; Rb, Ba, V, Nb in Bt; Sc, Y, HREE in Grt; Be in Crd. (4) Recrystallization of minerals in order also to equilibrate them with melt.

Provided that there is always enough heat available for melting (see below), the slowest process between interface reactions and diffusion in the melt will constitute the rate-limiting process during anatexis, and will control the proportion of melt. The bulk composition of melt will also depend on the interplay between interface reactions and diffusion in melt, though recrystallization of minerals and, to much lesser extent diffusion in minerals, may also play a role. The extent of melt homogeneity will be dictated by diffusivities in the melt. The extent of melt–residue equilibration, instead, will be controlled by the rates of diffusion in minerals, which are much slower than those for processes at interface reactions and diffusion in melt. However, if mineral recrystallization occurs, it will greatly accelerate the process by instantaneously equilibrating minerals and adjacent melt.

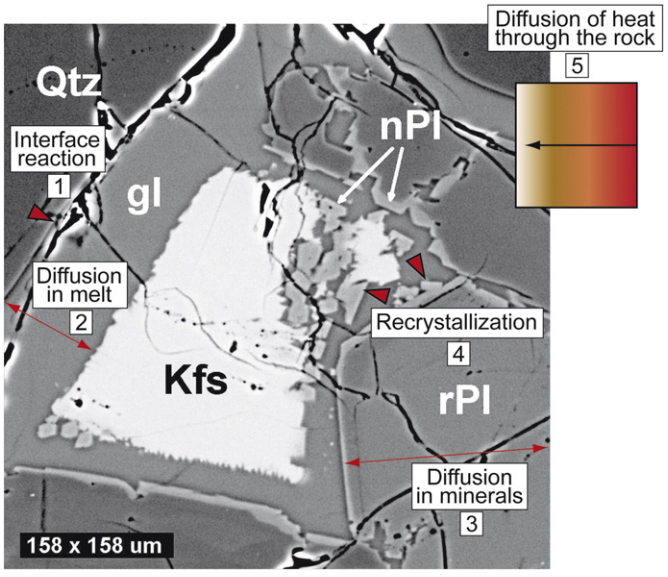

Fig. 3. BSE image of a 123-h, 800 °C H_2O-saturated aplite melting experiments (0.2 GPa), illustrating the five main processes that may occur from the very beginning of melting. The rate of heating determines the extent of overstepping of the melting reaction, which in turn partially controls the role of each of the other four processes (see text for details). rPl refers to relict Pl, nPl to new Pl, and gl to glass.
Modified after Fig. 5 of Acosta-Vigil et al. (2006a).

Another important process to consider is (5) the diffusion of heat through the protolith and its control on the rate of melting, modulated through the interplay between heating rate and the latent heat of melting. The geodynamic or geologic scenario determines the amount of heat that is available to diffuse through the rock, and hence the rate of heat supply during anatexis. This rate, in turn, determines the amount of heat that is available for melting, as melting reactions are endothermic. At low rates of heat supply, the diffusion of heat may control the rate of melting and melting may proceed very slowly or stop temporarily, even if the *P–T–X* conditions are appropriate for the melting reaction to proceed. Whereas, in cases of high rates of heat supply, the *T* during melting in the system may increase above that of the equilibrium melting *T*, hence producing some overstepping of the melting reaction. The extent of overstepping, in turn, is a key factor in determining the relative roles of processes (1) through (4) during anatexis (see below).

Two useful concepts in order to explore the extent and timing of melt–residue equilibration during anatexis include (Fig. 1b, c): the **equilibration volume**, or volume of the studied rock which, at some given *P* and *T* reacts to be in chemical equilibrium (Powell and Downes, 1990; Stüwe, 1997); and the **minimum volume for equilibrium**, or the smallest volume of rock that, when reaching chemical equilibrium at some given *P* and *T*, ensures also chemical equilibrium in the entire system. Chemical equilibrium in a rock will be established when the equilibration volume coincides with, or contains, the minimum volume for equilibrium.

Fig. 4 describes schematically how each of the processes (1) through (4) above may control the proportion, composition and homogeneity of melt, as well as the extent of melt–residue equilibration, before segregation of melt from its residue (see sections below). Initially, we assume a situation where the heat supply is infinite, such as to at least maintain the temperature of the system at an approximately constant value above the equilibrium melting *T*, as in the case of rock melting and mineral dissolution experiments conducted at constant *T*. In natural scenarios, this may correspond to crustal anatexis during intrusion of hot mantle magmas into the continental crust, or during the instantaneous influx of H_2O-rich fluids in rocks that were already well above their wet solidus. In these cases, the rate of heat supply is initially infinite, and the *T* of the system will be set rapidly to, though transiently, a value above the equilibrium melting *T*. We also assume H_2O-saturated and hydrostatic conditions. After evaluating the role of, and interplay among processes (1) through (4) at these conditions (Section 3), we will explore the main limitations to scaling experimental results up to natural

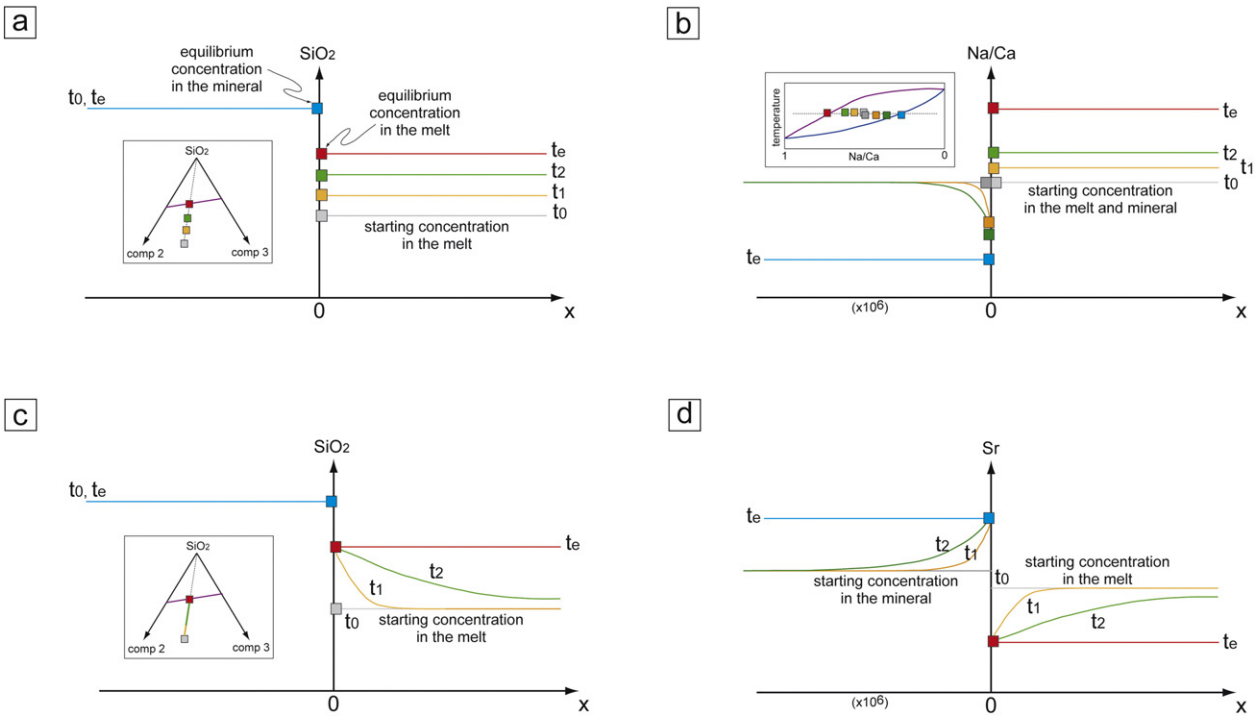

Fig. 4. Schematic concentration profiles across, and perpendicular to the interface between a granitic melt column ($x > 0$) and a dissolving mineral ($x < 0$), for the case of pure (e.g. Qtz; a, c) and solid solution minerals (e.g. Pl; b, d), and either during interface reaction-controlled melting (a, b) or diffusion in melt-controlled melting (c, d). Blue and red dots indicate the equilibrium concentrations in mineral and melt, respectively, of a given compositional parameter at the *P–T–X* conditions of melting. "t_0" refers to time at the onset of melting; "t_1" and "t_2" to progressively increasing times after t_0; "t_e" to the time when mineral and melt reach equilibrium; and "comp" to component. Insets in a, b and c show schematic phase diagrams showing the liquidus (purple line), solidus (dark blue line), starting mineral and melt compositions, and mineral and melt composition evolution with time. See text for explanation.

scenarios, e.g. how variations in size (spatial scale), rate of heat supply (temporal scale), a_{H2O} and the presence of differential stress may change the conclusions (Section 4).

2.1. Interface reaction-controlled melting

When the kinetics of **the reactions at the interfaces** are sluggish compared to diffusion in melt and even minerals, mineral components are liberated very slowly to the interface melt, and saturation of the melt in, and equilibration with, the minerals takes a long time, even at the interfaces. Diffusion in melt can be comparatively fast such as to entirely homogenize melt in the rock as dissolution and diffusion in minerals still proceed; this melt, however, is not at equilibrium with the residue (see below). In this situation, the interface reactions are the rate-controlling process regarding the proportion of melt, and also controls, together with diffusion in minerals, the bulk melt composition, whereas diffusion in the melt controls the extent of melt homogeneity (e.g. Liang, 1999; Shaw, 2004; Zhang et al., 1989). In the case of minerals that neither constitute solid solutions nor control the geochemistry of any trace element/isotope during anatexis, e.g. Qtz (Fig. 4a), the time frame for melt–residue equilibrium (i.e. Qtz saturation in the bulk melt) is also controlled by the kinetics of the interface reaction, and will likely coincide with the time when the equilibrium proportion of melt is generated. However, for the case of minerals that are solid solutions and/or minerals controlling the geochemistry of certain trace elements/isotopes, e.g. Pl (Fig. 4b), and in the absence of recrystallization, the time frames for melt–residue equilibration will be controlled by the rates of diffusion in the minerals. It is uncertain if interface reactions play any significant role during anatexis in Nature, though kinetic experiments suggest that they might be important during melting at low degrees of temperature overstep (Acosta-Vigil et al., 2006a; see below).

2.2. Diffusion in melt-controlled melting

When the rates at which interface reactions proceed are faster than the rates of diffusion in melt, mineral components are delivered quickly to the melt, which rapidly becomes saturated in, and reaches equilibrium with, the mineral at the interface. **Diffusion in the melt** is comparatively too slow to keep pace with interface reactions and carry quickly these mineral components away from the interface melt. This process is required to both homogenize the melt and to promote further mineral dissolution until mineral saturation in, and equilibration with the bulk melt is achieved. In this case, diffusion in the melt is the rate-controlling process that governs the proportion, extent of homogeneity and, largely, bulk composition of melt and, in the case of pure minerals with very low concentrations in trace elements (Fig. 4c), also the extent of mineral–melt equilibrium. For major minerals that constitute solid solutions and/or control the geochemistry of particular trace elements/isotopes (Fig. 4d), in the absence of recrystallization, it is again the rates of diffusion in minerals, which are significantly slower than diffusion in melt (Bea, 1996, and references therein; Table 1), that control equilibration time frames between minerals and melt (e.g. Liang, 2000, 2003).

2.3. Role of diffusion in minerals

Due to the relatively high temperatures, **diffusion in minerals** will continuously occur during high-grade metamorphism and crustal anatexis, and tends to erase any existing concentration gradient and to produce mineral–melt equilibrium distributions of major elements, trace elements and isotopes at the *P* and *T* of melting. Diffusion in minerals at crustal anatectic temperatures, however, is in general rather sluggish, particularly when compared to diffusion in the melt (e.g.

Table 1
Diffusivities in H_2O-saturated haplogranitic melt and appropriate minerals, at typical crustal anatectic temperatures, corresponding to either values published in the literature, or values calculated from data in the literature using the Arrhenius relation (see compilation in Brady and Cherniak, 2010).

Material	Observations	Diffusing component	Diffusivity at 800 °C	Diffusivities between 700–850 °C	References
Plagioclase	Ab(92) (exsolved 0/26); wet	NaSi–CaAl interdif	$5*10^{-23}$ m^2/s	$2*10^{-24}$–$2*10^{-22}$ m^2/s	Liu and Yund (1992)
	Peristerite (An0–An26); $XH_2O = 0.5$	NaSi–CaAl interdif	$4*10^{-22}$ m^2/s	$2*10^{-24}$–$4*10^{-21}$ m^2/s	Baschek and Johannes (1995)
	An(80) (exsolved 70/90); wet	NaSi–CaAl interdif	$4*10^{-21}$ m^2/s	$1*10^{-22}$–$2*10^{-20}$ m^2/s	Liu and Yund (1992)
	An(80) (exsolved 70/90); dry	NaSi–CaAl interdif	$8*10^{-29}$ m^2/s	$2*10^{-31}$–$1*10^{-27}$ m^2/s	Grove et al. (1984)
	An(67)	Sr	$8*10^{-21}$ m^2/s	$4*10^{-22}$–$3*10^{-20}$ m^2/s	Cherniak and Watson (1994)
	An(43)	Sr	$2*10^{-20}$ m^2/s	$1*10^{-21}$–$9*10^{-20}$ m^2/s	Cherniak and Watson (1994)
	An(23)	Sr	$4*10^{-20}$ m^2/s	$2*10^{-21}$–$2*10^{-19}$ m^2/s	Cherniak and Watson (1994)
	Ab(73)	Sr	$1*10^{-19}$ m^2/s	$7*10^{-21}$–$5*10^{-19}$ m^2/s	Giletti and Casserly (1994)
	Ab(98)	Sr	$3*10^{-18}$ m^2/s	$1*10^{-19}$–$1*10^{-17}$ m^2/s	Giletti and Casserly (1994)
Orthoclase	Or(94)Ab(6)	41K	$2*10^{-17}$ m^2/s	$4*10^{-18}$–$9*10^{-17}$ m^2/s	Foland (1974)
	Or(94)Ab(6)	22Na	$2*10^{-14}$ m^2/s	$5*10^{-15}$–$5*10^{-14}$ m^2/s	Foland (1974)
	Or(93)	Sr	$9*10$–21 m^2/s	$2*10$–21–$4*10$–20 m^2/s	Cherniak and Watson (1992)
Sanidine	Or(61)	Sr	$1*10^{-21}$ m^2/s	$9*10^{-23}$–$1*10^{-20}$ m^2/s	Cherniak (1996)
	Or(61)	Ba	$2*10^{-23}$ m^2/s	$2*10^{-24}$–$2*10^{-22}$ m^2/s	Cherniak (2002)
Garnet	Alm80Prp20–Sps94Alm6 couple	Fe–Mn	$3*10^{-21}$ m^2/s	$1*10^{-22}$–$1*10^{-20}$ m^2/s	Chakraborty and Ganguly (1992)
	Alm–Grs couple	Ca-(Mg,Fe) interdif	$9*10^{-20}$ m^2/s	$4*10^{-21}$–$3*10^{-19}$ m^2/s	Freer and Edwards (1999)
	Alm(51)Prp(45)Grs(3)	Ca-(Mg,Fe) interdif	$5*10^{-23}$ m^2/s	$5*10^{-24}$–$1*10^{-22}$ m^2/s	Vielzeuf et al. (2007)
	Alm with polycrystalline Prp	Ca	$3*10^{-22}$ m^2/s	$1*10^{-23}$–$1*10^{-21}$ m^2/s	Perchuk et al. (2009)
	Alm with polycrystalline Prp	Fe	$3*10^{-21}$ m^2/s	$1*10^{-22}$–$1*10^{-20}$ m^2/s	Perchuk et al. (2009)
	Alm(38)Prp(50)Gr(10)Sp(2)	Mg	$2*10^{-21}$ m^2/s	$1*10^{-22}$–$6*10^{-21}$ m^2/s	Chakraborty and Rubie (1996)
	Spessartine–almandine garnets	Mn	$4*10^{-19}$ m^2/s	$4*10^{-20}$–$1*10^{-18}$ m^2/s	Loomis et al. (1985)
	Grs(93)	Y	$7*10^{-23}$ m^2/s	$2*10^{-24}$–$3*10^{-22}$ m^2/s	Cherniak (2005)
	Alm(16)Prp(71)Grs(13)	Dy	$2*10^{-24}$ m^2/s	$6*10^{-26}$–$8*10^{-24}$ m^2/s	Van Orman et al. (2002)
	Gr(93)	Yb	$5*10^{-22}$ m^2/s	$1*10^{-23}$–$2*10^{-21}$ m^2/s	Cherniak (2005)
	Alm(16)Prp(71)Grs(13)	Yb	$4*10^{-25}$ m^2/s	$7*10^{-27}$–$2*10^{-24}$ m^2/s	Van Orman et al. (2002)
Haplogranitic melt	H_2O-saturated	Si	$2.5*10^{-15}$ m^2/s		Acosta-Vigil et al. (2006b)
		Al	$1.5*10^{-14}$ m^2/s		Acosta-Vigil et al. (2002)
		Ca			Acosta-Vigil et al. (2012a)
		Na	$\geq 1*10^{-8}$–$1*10^{-9}$ m^2/s		Morgan et al. (2008)
		K	$\geq 1*10^{-8}$–$1*10^{-9}$ m^2/s		Morgan et al. (2008)
		H	$4*10^{-11}$ m^2/s		Acosta-Vigil et al. (2005)
		Fe	$1*10^{-13}$ m^2/s		Acosta-Vigil et al. (2012a)
		Mg	$2*10^{-13}$ m^2/s		Acosta-Vigil et al. (2012a)

Bea, 1996; Brady and Cherniak, 2010; Zhang et al., 2010, and references therein; Table 1) and published time frames of melt segregation/extraction (e.g. Harris et al., 2000; Sawyer, 1991; Villaros et al., 2009a). For instance, for common grain sizes in high-grade metamorphic rocks of ≈1 mm, 5 mm or 10 mm, at 800 °C, diffusion will take long to extremely long time frames to homogenize Ca–Na in Pl (≥10 Ma in all cases; diffusivities from Baschek and Johannes, 1995; Liu and Yund, 1992); ≈0.1, 3 or 10 Ma, respectively, to homogenize Sr in Pl (diffusivities from Cherniak and Watson, 1994); variable time frames to homogenize Fe–Mg–Ca in Grt, depending on size and reported diffusivities (e.g. ≈2, 50, 200 Ma, respectively, with likely longer time frames for Ca; using intermediate diffusivities from Chakraborty and Ganguly, 1992; Perchuk et al., 2009); and long to extremely long time frames to homogenize Y and HREE in Grt (≥10 Ma in all cases; diffusivities from Cherniak, 2005; Van Orman et al., 2002). Frequent examples of compositional zoning in residual and peritectic minerals of migmatites (e.g. Ca–Na in Pl, even if weak: Sawyer, 1998, 2008; Ca and Y-HREE in Grt: Anczkiewicz et al., 2014; Barich et al., 2014; Hermann and Rubatto, 2003; Spear and Kohn, 1996) testify that, during anatexis, melt does not commonly equilibrate with, at least, the bulk residue, and hence that diffusion in minerals is a key rate limiting factor for equilibration, not only regarding the trace elements (Bea, 1996) but also the major elements. In this respect, the systematic study of plagioclase compositions (in the protolith — if available — versus the melanosome versus the leucosomes) constitutes one key monitor of the major element melt–bulk residue equilibration (Johannes, 1980; Mehnert, 1968; Sawyer, 2008). Large An/An + Ab differences between melt and residual plagioclase are expected during crustal anatexis at equilibrium (e.g. in the Qtz–Or–Ab–An–H_2O–CO_2 system; Johannes and Holtz, 1992). Similar or slightly Ab-richer compositions of igneous versus residual plagioclase in migmatites (e.g. Carvalho et al., 2016; Mehnert, 1968; Sawyer, 1998, 2008), hence, seem to overall indicate anatexis under disequilibrium conditions regarding the major elements, or at least the partitioning of Na–Ca between melt and residue. Other explanations, e.g. Pl homogenization at low cooling rates and high H_2O activities during the late stages of migmatite genesis (Johannes and Holtz, 1992), seem less likely given the long time frames required (see above).

2.4. Role of recrystallization

Mineral recrystallization, whatever the reaction mechanism (e.g. through dissolution into, and reprecipitation from the melt at the boundary; Johannes and Koepke, 2001), can proceed at much faster rates than diffusion in minerals, and hence produce equilibration between minerals and (adjacent) melt much more rapidly. Therefore, it can have an important role in determining the composition of primary anatectic melts, the extent of melt–residue equilibration and, coupled with melt extraction, on the nature of crustal differentiation. Despite this, there are few studies that provide information on this topic (Acosta-Vigil et al., 2006a; Icenhower and London, 1995; Johannes, 1980, 1989; Johannes and Holtz, 1992; Johannes and Koepke, 2001; Nakamura and Shimakita, 1998; Villaros et al., 2009b), and hence our current understanding of the circumstances and rates at which different minerals recrystallize during anatexis is still rather poor. London et al. (2012) have used experiments to qualitatively assess the efficiency of recrystallization to equilibrate residual minerals and coexisting melts. In general, minerals of low density (quartz, feldspars) or with large intercrystalline channels or layer spacing (micas, cordierite), can re-equilibrate at rates on the scale of the experiments, in days to months, whereas denser phases (garnet, spinel) are more refractory, even when their compositions are far from the equilibrium with the melt. Some detailed studies in diatexites, however, have documented two different compositional groups of biotites, interpreted as crystals either residual or crystallized from the melt; the residual biotites may appear trapped within leucosomes (Carvalho et al., 2016; Sawyer, 1998).

3. Information from kinetics experiments: interplay among, and imprint of processes

3.1. Mineral dissolution and rock core melting experiments: role of reaction overstepping

3.1.1. Melting at low degrees of overstepping

Experiments where a macroscopic solid core of fine-grained granite (diameter ≈3.5 mm, length ≈7 mm, mean grain size ≈0.3 mm) is partially melted via the wet granite solidus show that, at relatively low degrees of *T* overstepping of the melting reaction (≈10 to 60 °C; with an infinite supply of heat, see above), and from the shortest experimental time (18-h experiment, showing ≤5 vol% of melt), melt occupies most grain boundaries — most triple junctions and Qtz–Pl, Qtz–Or boundaries, but to a lesser extent the Pl–Kfs, Qtz–Qtz boundaries — and forms an interconnected network (Fig. 5a). This distribution of melt, showing effective dihedral angles of zero, corresponds to a reaction-controlled microstructure (e.g. Holness, 2010; Holness and Sawyer, 2008). Melt composition is rather homogeneous, quite close to (≈0–10 wt% CIPW normative away from) the corresponding haplogranite minimum, and constant from the shortest (18-h) to the longest (4-month) experiments. The melt proportion increases from ≈3–4 vol% (18-h experiment) to ≈20–25 vol% (3–4-month experiment). During this time span residual minerals (Pl, Kfs) show compositions similar to those in the starting material and are not in equilibrium with the melt, likely not even at the interfaces (Acosta-Vigil et al., 2006a). These results are in accordance with a situation where mineral components added to the melt have enough time to diffuse across the small distances among crystals and homogenize the melt, but interface reactions are too sluggish to allow mineral–melt equilibration even at the interfaces (see above, and Fig. 4a, b). The kinetics of the interface reactions, therefore, control the rate of melt production (and thus length scales of diffusion in melt) and time frames of melting. Diffusion in the melt, instead, controls the extent of melt homogeneity. Hence during

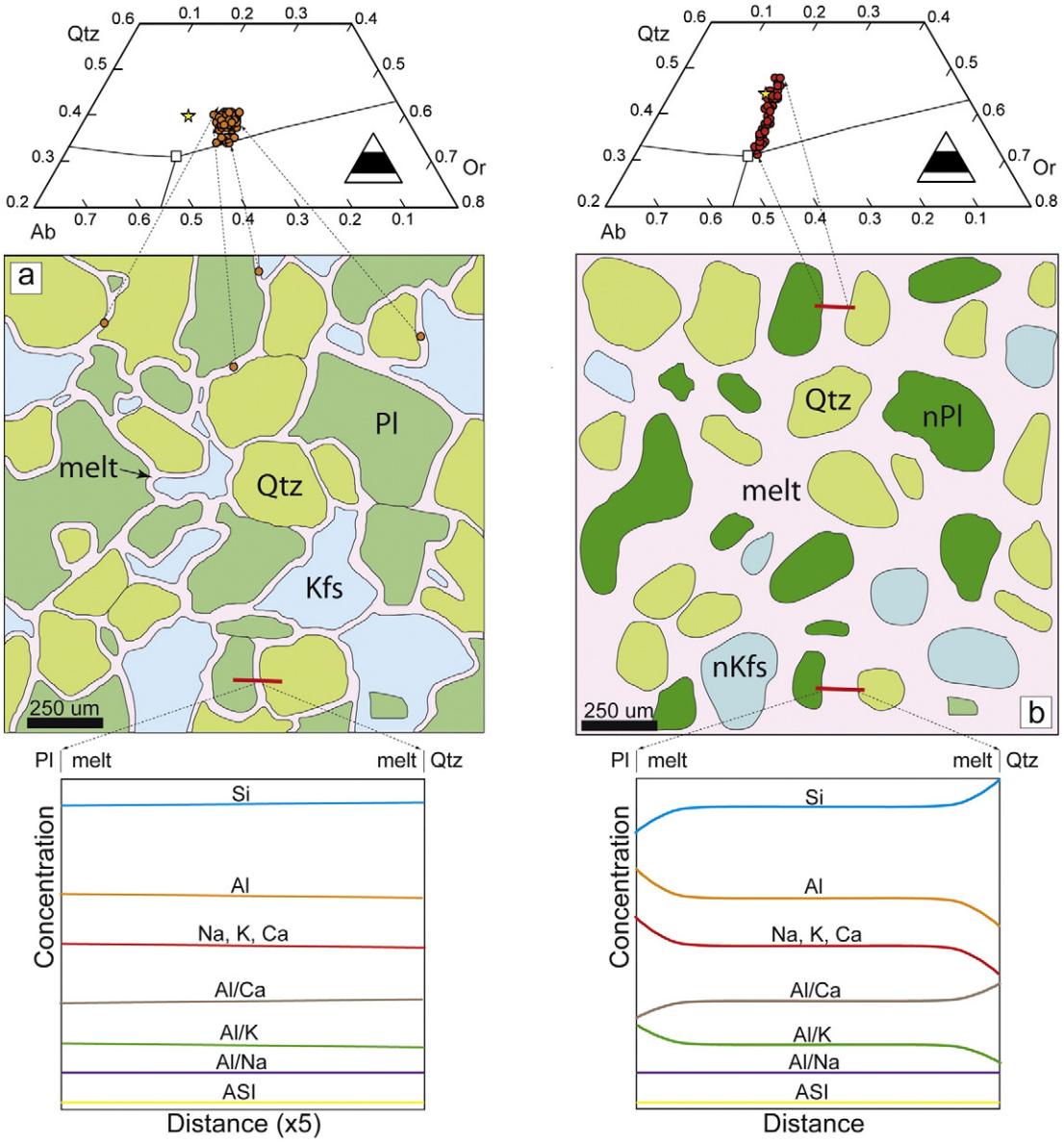

Fig. 5. Schematic representation of the Qtz–Pl–Kfs fine-grained homogeneous aplite of Fig. 1b, partially melted at (a) low degrees of *T* overstepping and (b) high degrees of *T* overstepping. Note that recrystallization of residual minerals is extensive during anatexis and high degrees of overstepping. nPl and nKfs refer to the new recrystallized Pl and Kfs, respectively. Insets show schematically the Qtz–Or–Ab normative compositions of melt in several microstructural locations (upper insets) and compositional profiles of melt between residual Pl and Qtz of melt (lower insets). White squares in upper insets show melt eutectic compositions in the H_2O-saturated haplogranite system at *P* of melting, whereas yellow stars show melt equilibrium compositions at the *P-T-X* of melting. See Section 3 for explanation.

melting at low degrees of *T* overstepping, and for the specific case of fine-grained and homogeneous protoliths (Fig. 1b), the first melts produced will be homogeneous, very close to the minimum melt composition but out of equilibrium with the residue. Under conditions of infinite heat supply, the rate of melting is high (≈20–25 vol% in 3–4 months) and, therefore, it is reasonable to assume that equilibrium between melt and non-solid solution minerals with very low concentrations of trace elements (e.g. Qtz) should be quickly established. However, melt–residue equilibration regarding solid solution minerals and/or minerals with high concentrations of trace elements will involve longer time frames, as it is controlled by diffusion in the minerals. Equilibrium between certain minerals/elements and the melt will not likely be achieved, for instance Pl with respect to Na–Ca or Grt with respect to Y-HREE. Depending on diffusivities and grain size, other minerals/elements may partially or totally equilibrate with the melt, e.g. Sr in Pl (see above). Therefore in this case, and during the experimental time frames, we might consider that the equilibration volume corresponds to the volume of melt produced, as this melt is mostly homogeneous (Fig. 5a). During geologic time frames, some minerals/elements may join the equilibration volume (e.g. pure minerals such as Qtz that may achieve saturation in the melt, or Pl with respect to Sr), but in general the equilibration volume will not coincide with, or contain, the minimum volume for equilibrium, because of the general sluggish diffusivities of elements in minerals (compare Figs. 1b and 5a; Table 1).

3.1.2. Melting at high degrees of overstepping

Single mineral (Qtz, Ab, Kfs, Crn, And) dissolution experiments into haplogranite melt and granite core melting experiments where, at a given *P*, the experimental *T* was set to ≥100 °C above the equilibrium *T*, show that melting occurs very rapidly (e.g. ≈50 wt% of melt generated in ≈15 days during core melting experiments) and, also, that minerals and interface melt reach chemical equilibrium rapidly, after ≈15–20 days. However, melt is heterogeneous from the shortest experimental time, away from (up to 20 wt% off) the haplogranite minimum, and does not homogenize within experimental time frames, even in the longest 6-month experimental run. Furthermore, in the core melting experiments melt forms an interconnected network (Fig. 5b) even in the shortest 11-h experiment (Acosta-Vigil et al., 2002, 2006a, 2006b). These results are in accordance with a scenario where the kinetics of mineral–melt interface reactions are quite fast, and diffusion in the melt is the rate-limiting process that controls the rates of melt generation and homogenization (see above, and Fig. 4c, d). Hence, during melting at high degrees of *T* overstepping, and even for the case of fine-grained and homogeneous protoliths (Fig. 1a), the first melt produced will be heterogeneous simply because melting is rapid enough to create long diffusion paths in melt which, for the short experimental time scales and given diffusivities in granitic liquids, do not enable melt to homogenize.

Mineral–melt equilibrium is rapidly achieved at the interfaces. It is important to note that, during melting at high degrees of overstepping, and in contrast with the previous case, recrystallization of the residue occurs concomitantly with anatexis. In the particular case of the granite core melting experiments, Ab-rich Pl is the only solid solution and trace element-bearing major mineral coexisting with the melt (Kfs and Bt disappeared at the beginning of melting), and it recrystallized in the time frame of days to months to an An-richer Pl, apparently at or closer to equilibrium with the surrounding melt (Acosta-Vigil et al., 2006a). This implies that bulk melt–residue equilibration will be achieved much faster than during melting at low degrees of *T* overstepping, and possibly during the time frames of anatexis in Nature. The reason for this is that recrystallization establishes instantaneously equilibrium distributions of elements between minerals and surrounding melt, and hence diffusion in melt will be the process responsible for both melt homogenization and bulk melt–residue equilibration. The equilibration volume during experimental time frames corresponds to the mineral–melt interfaces, as minerals and melt reach equilibrium along these after some tens of days. For the most favorable case of a fine-grained homogeneous protolith where, in this particular case, the minimum volume for equilibrium corresponds to a cube with a length of size ≈1–2 mm (Fig. 1b), the equilibration volume will contain the minimum volume for equilibrium only after Si, the slowest diffusing component in the melt, homogenizes within this ≈1–8 mm^3 cube, i.e. in tens of years to a few hundred of years (Acosta-Vigil et al., 2012a; Fig. 6; see below). Hence chemical equilibrium is likely to be reached during geologic time frames. Equilibration time frames, however, increase considerably for the case of heterogeneous protoliths, e.g. up to 1–10 Ma if the source area shows a compositional banding at the scale of ≈50 cm, because in this case the minimum volume for equilibrium may correspond to a cube/polyhedron with a length of side ≈1 m (Figs. 1d, 6; see Acosta-Vigil et al., 2012a, for time frames of equilibration at other length scales).

3.2. Diffusion experiments in granitic melts: diffusion controls on primary melt composition

During melting at high degrees of overstepping, the proportion and composition of melt, and the extent of bulk melt–residue equilibration from generation to segregation/extraction, is controlled by the diffusion properties of the melt. Experimental melt is heterogeneous from the very beginning of anatexis (hours) to the longest run (months): melt produced next to Qtz has the highest Si concentrations and Al/Ca molar ratios, and lowest Al, Ca, Na, K concentrations and Al/K molar ratios. Whereas melt produced next to either Pl or Kfs has the highest Al, Ca, Na, K and Al/K, and lowest Si and Al/Ca. Surprisingly, the Al/Na molar ratio is similar in melts next to Qtz, Kfs and Pl (Figs. 7 and 9 of Acosta-Vigil et al., 2006a). Although during melting of crustal rocks some of the above compositional features are expected (e.g. Si concentrations highest next to Qtz, or Al highest next to feldspars), others are not (e.g. highest Al/K molar ratios next to Kfs, or similar Al/Na molar ratios in all microstructural locations). This is due to the fact that oxide components do not diffuse independently of each other in granitic melts, and hence melt homogenization does not occur as a simple mixture between compositional poles. Rather, it entails fractionation among the several melt components dictated by the systematics of diffusion in the melt. Because to a greater or lesser extent diffusion in the melt does control melt compositions during anatexis between melt generation and its extraction, it is important to know the systematics of diffusion in granitic melts, in order to interpret for example the compositions of analyzed MI within peritectic minerals, leucosomes in anatectic terranes, or extent and systematics of interaction between materials (two different magmas, or a magma and reactive neighboring rocks) in the highly heterogeneous continental crust. Below we first introduce some concepts, including the new notion of "field diffusion", which are key for understanding these diffusion systematics, and then explain the constraints that these diffusion properties of granite melt impose on the compositions of primary anatectic melts.

3.2.1. Diffusion coupling and uphill diffusion; local diffusion versus field diffusion

One important and common complexity of chemical diffusion in multicomponent systems is that the set of components that we arbitrarily choose, i.e. the oxide constituents, may not diffuse independently of each other due to structural, charge balance and/or volume constraints. This is referred to as **diffusion coupling** between, or coupled diffusion of, components. Thus, in order to describe the diffusion properties of a N-component system at some given *P–T–X* conditions, a N-1 by N-1 diffusion matrix, [D], must be provided. Referred to the oxide components reference frame, the eigenvectors of [D] provide the stoichiometries of a new set of N-1 components, which are expressed as linear combinations of the "old" oxide components, that diffuse independently of each other, i.e. that uncouple chemical diffusion. Thus, the Al-eigenvector represents the direction in the oxide

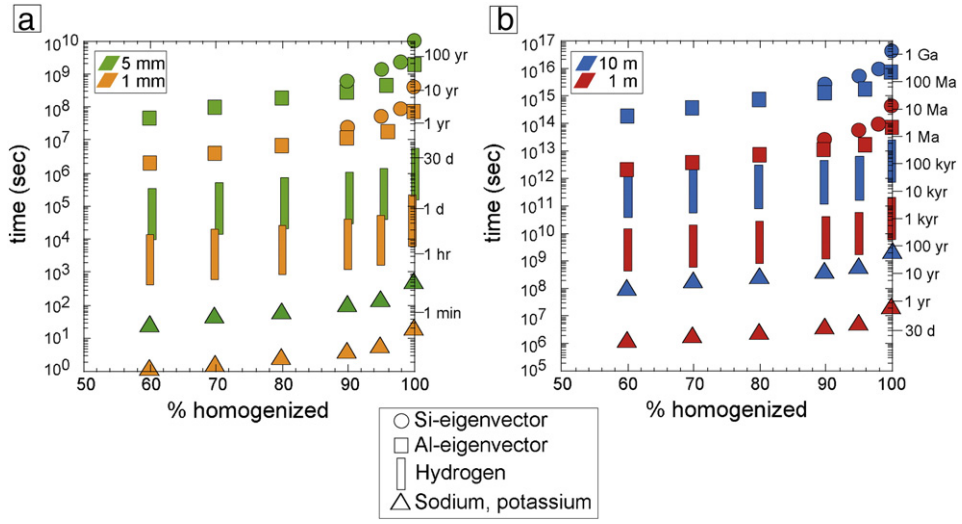

Fig. 6. Calculated time necessary for different degrees (60 to 100% relative) of compositional homogenization of crustal anatectic melts, as a function of minimum volume for equilibrium and diffusion distances involved [in this case for length scales of diffusion of 1–5 mm (a) or 1–10 m (b)], and for the several components in the haplogranite system and their corresponding diffusivities calculated at 800 °C and 200 MPa H_2O.
Modified after Fig. 9 of Acosta-Vigil et al. (2012a).

composition space along which Al erases its chemical gradients, even if that means that concentration gradients in other oxide components, that are coupled with the diffusion of Al, are temporarily created. This is referred to as **uphill diffusion** of these other oxide components, i.e. diffusion against its own concentration gradient, which constitute an expression of diffusion coupling. The eigenvalues of [D], instead, furnish the diffusivities of each of these new set of N-1 independently diffusing components. As [D] is not known a priori for a given system and *P–T–X* conditions, eigenvectors and eigenvalues of [D] are obtained by inversion of experimentally produced oxide diffusion concentration profiles (e.g. Chakraborty, 1995; Liang, 2010).

A new concept regarding the scale and mechanisms of diffusion in (granite) melts is the distinction between local diffusion and field diffusion (Acosta-Vigil et al., 2012a; London, 2009; Morgan et al., 2008). **Local diffusion** corresponds to the classical description of diffusion, based on previous modeling of heat transfer, and visualized as the random and relative motion of components in the system, under apparently local chemical gradients, whose associated concentration profiles show, for constant diffusion coefficients, exponential "tails" that can be described by the available solutions of the Fick's empirical diffusion equations (e.g. Crank, 1975). Consequently, local diffusion does not imply any kind of large-scale chemical connection in the melt. Diffusion length scales associated with the local diffusion of a particular melt component would correspond to the maximum migration distances of individual atoms of this component. To illustrate this point, we consider the diffusion of Al in melt due to the presence of a local concentration gradient next to a dissolving corundum crystal that is undersaturated in, and providing Al atoms to, the melt (Fig. 7a). The diffusion of Al occurs by local diffusion (see below) and is restricted to the volume where the local concentration gradient in Al exists. Thus, if we could label in red color the atoms of Al present in melt that are coming from the dissolving Crn, and considering the oversimplication that to erase the associated Al chemical potential gradient only the red atoms will diffuse, it would be observed that changes in concentration of Al at any point along the diffusion path perpendicular to the Crn–melt interface, only occur after the arrival of "foreign" red Al atoms coming from the dissolving Crn. As in all previous experimental studies of chemical diffusion in (granite) melt, we have observed that diffusion profiles of Si, Al and H are satisfactorily explained by this mechanism (see below).

Morgan et al. (2008) proposed the term **field diffusion** to explain the extremely high mobility of Na and K in granite melts observed in diffusion studies by Acosta-Vigil et al. (2002, 2006a, 2006b, 2012a) and Morgan et al. (2008). These authors envisage that such high mobilities could be explained by the coordinated and contemporaneous migration of all atoms of a given component (Na and/or K) present in the entire melt reservoir, driven by a long-range concentration (or chemical potential) gradient. Even if migration distances of the individual atoms are small, the coordinated migration of all atoms produces an apparently long-range migration of that component. Thus, field diffusion is capable of erasing compositional gradients or changing melt composition at rates that are several orders of magnitude greater than local diffusion, among other things because the effect of a coordinated movement of all individual atoms of a given component in the system, is to produce changes in concentration over distances that span the entire liquid, even though each individual atom moves only a small fraction of the size of the system. In addition, as the chemical gradient extends over the entire melt reservoir, this mechanism implies a *geologically (and even experimentally) instantaneous chemical connectivity and change in composition across the entire system*, which is important when considering the controls on melt composition in migmatites during anatexis (Acosta-Vigil et al., 2006a; London et al., 2012; see below) or in magmas during crystallization (London, 2008, 2014). Considering the previous example, during dissolution of Crn into, and establishment of an Al concentration gradient at the interface melt by local diffusion (Fig. 7a), the systematics of diffusion are such that Na diffuses uphill towards the interface due to coupled diffusion with Al, in a way that its concentration changes instantaneously (in hours) throughout the entire melt reservoir, ≈1 cm in length, to maintain the Al/Na molar ratio constant in the melt (see below). Hence we envisage that there is a coordinated and contemporaneous migration towards the interface of all atoms of Na in the melt. Thus, if we could label (as blue) a single atom of Na present at some point along the diffusion profile (Fig. 7b), the migration distance of this atom would be extremely small compared to the apparent diffusion length scale associated with the change in concentration of this component observed in the system. For more information on the phenomenon of field diffusion, readers are referred to Acosta-Vigil et al. (2002, 2006b, 2012a), Morgan et al. (2008), London (2009) and London et al. (2012); for a comparison with previous explanations on the systematics of alkali diffusion in silicate melts, see Acosta-Vigil et al., 2012a.

In the next sections we summarize the information on the diffusion systematics of granite melts, that help to understand the controls that diffusion in melt may have on the composition of primary anatectic melts. This information comes from several types of diffusion experiments

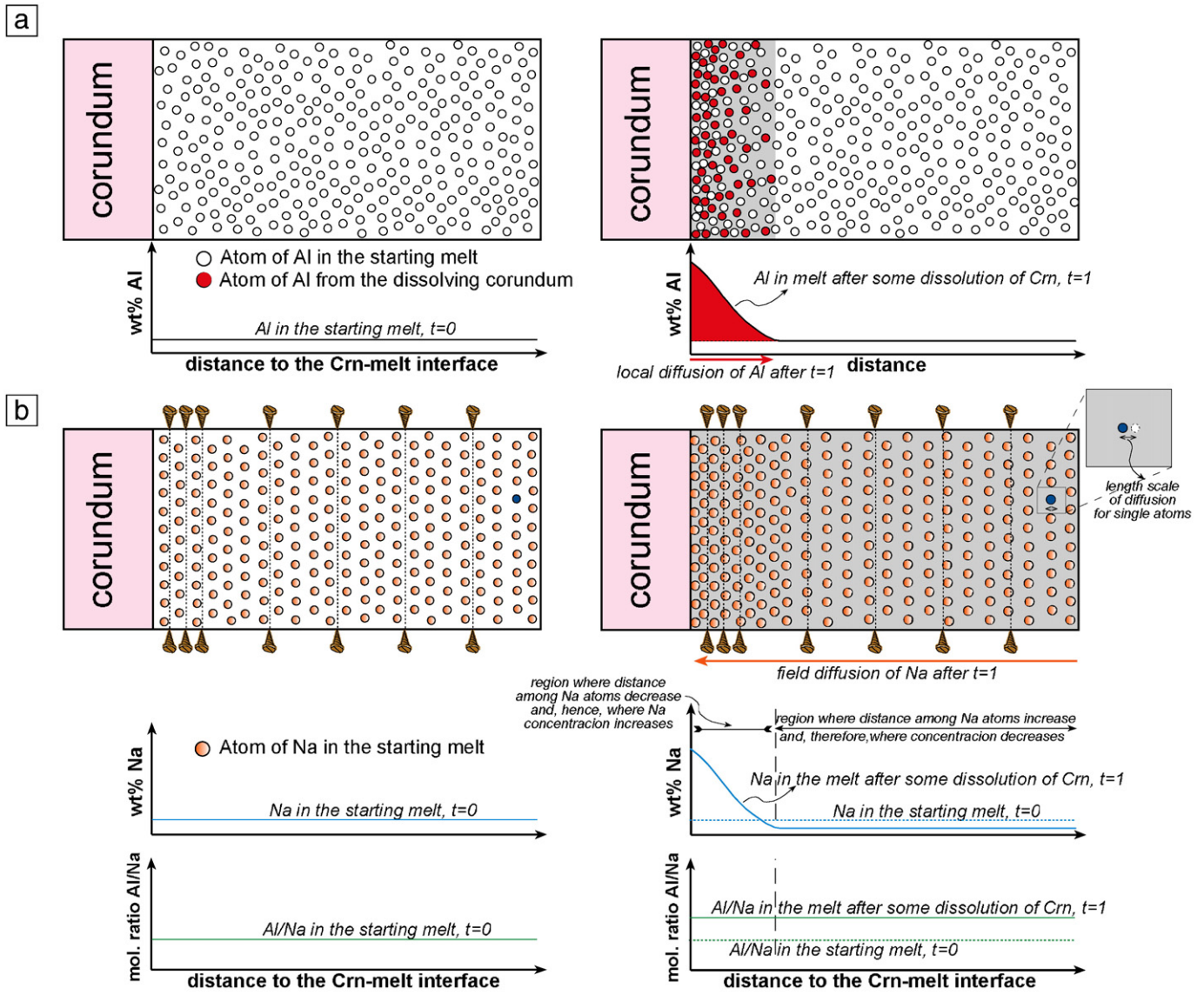

Fig. 7. Cartoons showing the difference between (a) "local diffusion" of Al and (b) "field diffusion" of alkalis (Na in this case) during the dissolution of corundum into haplogranite melt. Shaded areas and red and orange arrows indicate the melt region and direction, respectively, in which local diffusion of Al (red) and field diffusion of Na (orange) takes place. Profiles of concentrations and atomic ratios along traverses in the melt perpendicular to the corundum–melt interface are also shown. Vertical dashed lines in (b) represent fixed spatial references in the melt column. See text for details.
Modified after Fig. 5 of Acosta-Vigil et al. (2012a).

(mineral dissolution, glass hydration-melting and diffusion couples) conducted in the H_2O-saturated, 5-component haplogranite system at 800 °C and 0.2 GPa. These experiments provide part of a 4×4 diffusion matrix, including directions of uncoupled diffusion and diffusivities along some of them. Other information consists of effective binary diffusion coefficients (EBDC; Cooper, 1968), or diffusivities along directions in composition space that do not correspond to any of the directions of uncoupled diffusion.

3.2.2. Diffusion of Si

Silica diffuses independently of the other cations with a diffusivity of $\approx 2.5 \times 10^{-15}$ m^2/s, making it the slowest diffusing component in the system. Hence other cations are not coupled with the diffusion of Si, and Si represents one of the directions of uncoupled diffusion in composition space (Si-eigenvector; Acosta-Vigil et al., 2006b; see also Baker, 1991; Mungall et al., 1998). This is shown in Fig. 8, where concentration profiles represent the results from electron microprobe (EMP) traverses in glass (former melt) perpendicular to a Qtz–haplogranite melt interface after some Qtz diffusive dissolution at 800 °C, 0.2 GPa H_2O, and two months of run time. At increasing experimental times Qtz and the interface melt reached equilibrium, the Si diffusion front progressively displaced away from the interface, and all other oxides components were diluted, with their molar ratios being constant and similar to those in the starting melt [see Figs. 4, 11 of Acosta-Vigil et al. (2006b)]. During these experiments most of the diffusion in melt was accomplished by Si, which after two months migrated ≈300–400 μm from the interface by local diffusion. Hence Si diffusion occurred in response to the local Si concentration gradients produced at the interface after Qtz dissolution, and Si diffusion length scales were similar to maximum migration distances of single atoms of Si, producing local changes in composition.

3.2.3. Diffusion of Al

Alkalis are strongly coupled with, and assist the diffusion of Al in H_2O-saturated haplogranitic melt. Hence a combination of Al, Na and K constitutes another direction of uncoupled diffusion in composition

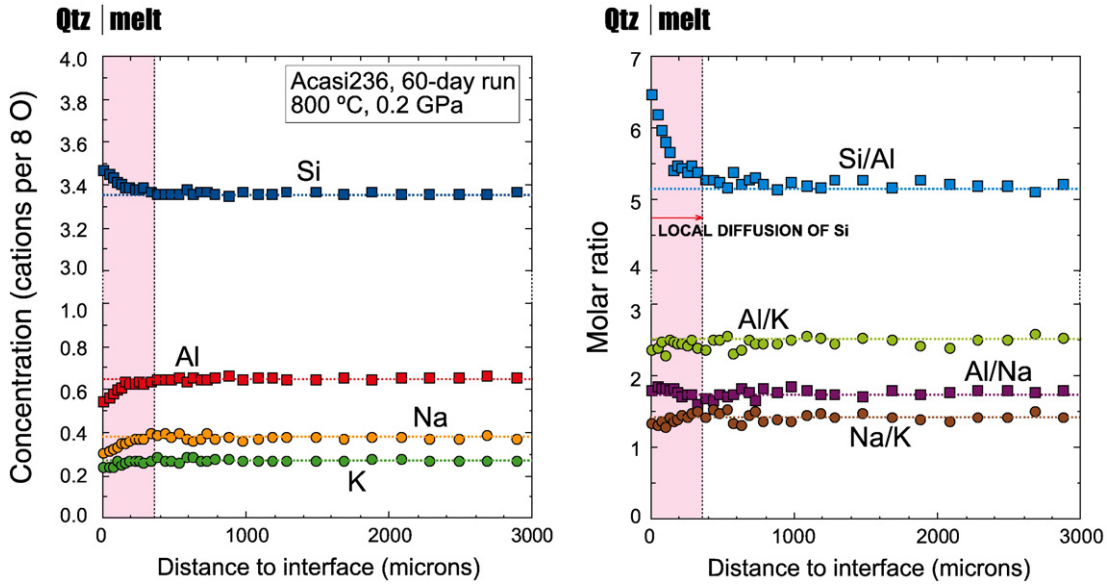

Fig. 8. Composition of glasses after the quartz dissolution experiment Acasi-236, as a function of distance to the quartz–glass interface (see Acosta-Vigil et al., 2006b). In this and following figures, each concentration profile represents the mean values of three analytical traverses perpendicular to the interface; the dashed lines refer to concentrations or molar ratios of a given element in the starting melt; pink area and red arrow indicate the melt region and direction, respectively, in which local diffusion of a particular element takes place. See text for explanation.

space, along which Al erases its concentration gradients in the melt (Al-eigenvector; Acosta-Vigil et al., 2002; see also Chakraborty et al., 1995; Mungall et al., 1998). Diffusivity along the Al-eigenvector, $\approx 1.5 \times 10^{-14}$ m^2/s, is the second slowest in the system at the investigated conditions. In order to homogenize Al in the melt, therefore, alkalis diffuse concomitantly to, and follow Al. This is shown in Fig. 9, where concentration profiles show results from EMP traverses in melt after some diffusive dissolution of Crn (pure Al_2O_3) into an originally metaluminous (ASI ≈ 1.0) H_2O-saturated haplogranitic melt occurred (at 800 °C, 0.2 GPa, 4 months of run time; Acosta-Vigil et al., 2002). Compared with the starting melt composition, the interface melt shows an increase of Al and, also, of Na and K; hence alkalis have diffused uphill towards the interface and against their own concentration gradients, in order to couple with Al released into the melt by dissolution of Crn. During the experiment Al diffuses in the vicinity of the interface by local diffusion (as in the case of Si), in response to the local Al concentration gradient produced after dissolution of Crn. This is shown by the observation that, beyond the Al diffusion front, the Al/Si molar ratio and Si and Al concentrations are similar to those in the starting material. Instead, alkalis diffuse throughout the entire melt reservoir; this is demonstrated by the increase in ASI (from ≈1.00 to 1.10) and decrease in concentrations of Na and K (compared to those in the starting material) at the far end of the melt reservoir, at locations where Al from the dissolving Crn has not arrived yet. This *necessarily indicates a different mechanism of diffusion for alkalis with respect to the local diffusion of Si or Al*, which has been named "field diffusion"

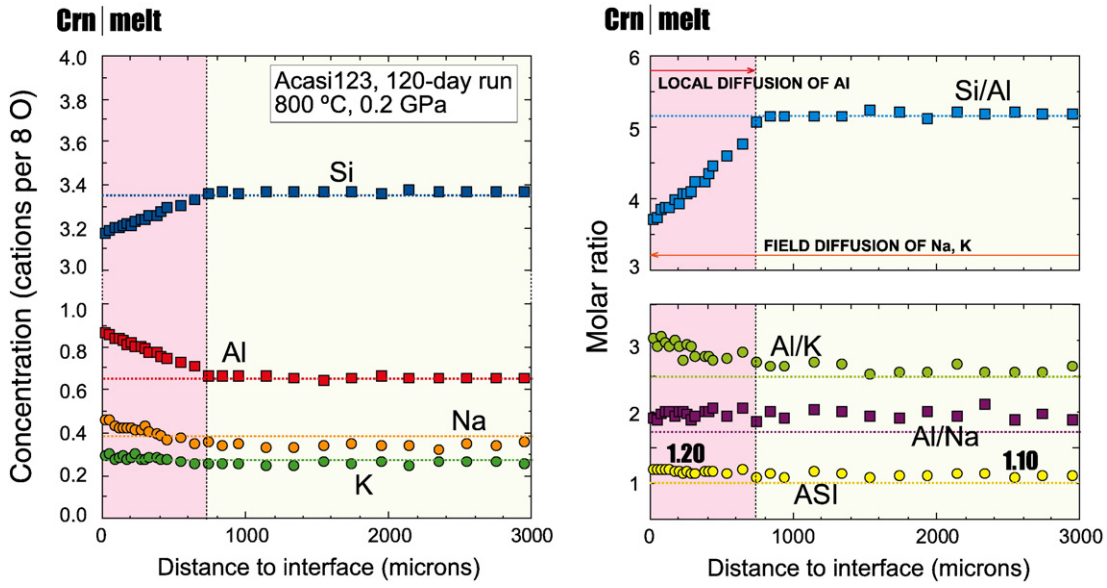

Fig. 9. Composition of glasses after the corundum dissolution experiment Acasi-123, as a function of distance to the corundum–glass interface (see Acosta-Vigil et al., 2002). In this and following figures, pink + light yellow area and orange arrow indicate the melt region and direction, respectively, in which field diffusion of a particular element takes place.

(Morgan et al., 2008). According to this mechanism, all Na and K atoms in melt migrate simultaneously and in coordination small distances in response to a long-range chemical gradient, in this case produced by addition of Al at the melt interface. Even though individual atoms migrate small distances, simultaneous movement of all atoms produces a noticeable long-range change in the concentration of Na, K and ASI values throughout the entire melt reservoir (see above). Thus, Fig. 9 shows that after four months of diffusive Crn dissolution into the melt, Al atoms coming from the Crn have migrated up to ≈700–800 μm away from the interface via local diffusion, whereas in the same time alkalis have migrated throughout the entire melt column (in this case 3 mm in length) by field diffusion.

One important observation is that diffusion of Na during the Crn dissolution experiments is such that the Al/Na molar ratio is maintained constant throughout the entire melt reservoir (varying between 3 and 6 mm in length) at all experimental run times, from 12 h to 4 months (Fig. 9, and Fig. 7 of Acosta-Vigil et al., 2002). This means that (i) diffusion of Na seems apparently instantaneous even at experimental time frames (see below), and (ii) the stoichiometry of the Al-eigenvector (i.e. proportions of Al, Na and K diffusing together) is such that its Al/Na molar ratio is similar to that of the bulk melt. In addition, some experiments have also shown that the proportion of K in the Al-eigenvector is such that the ASI of this diffusing species is equal to the equilibrium ASI of the melt at the investigated *P–T–X* conditions (Fig. 8 of Acosta-Vigil et al., 2002; Figs. 2, 3 of Morgan et al., 2008).

3.2.4. Diffusion of H

Alkalis are also strongly coupled with the diffusion of H in haplogranitic melt. A combination of H, Na and K constitutes another direction of uncoupled diffusion in the system (H-eigenvector; Acosta-Vigil et al., 2005). Hence, in order to homogenize H in melt, Na and K diffuse concomitantly with H. Because H concentration gradients in melt are rapidly erased, the diffusivity along the H-eigenvector must be several orders of magnitude faster than along the Si- or Al-eigenvectors. Nevertheless, Acosta-Vigil et al. (2005) were only able to provide an EBDC of $\approx 4 \times 10^{-11}$ m^2/s at 800 °C, 0.2 GPa and ≈5 wt% H_2O in melt, along the compositional direction H_2O–dry haplogranite. The strong coupling of alkalis with the diffusion of H is shown in Fig. 10, recording concentration profiles in melt during the progressive experimental

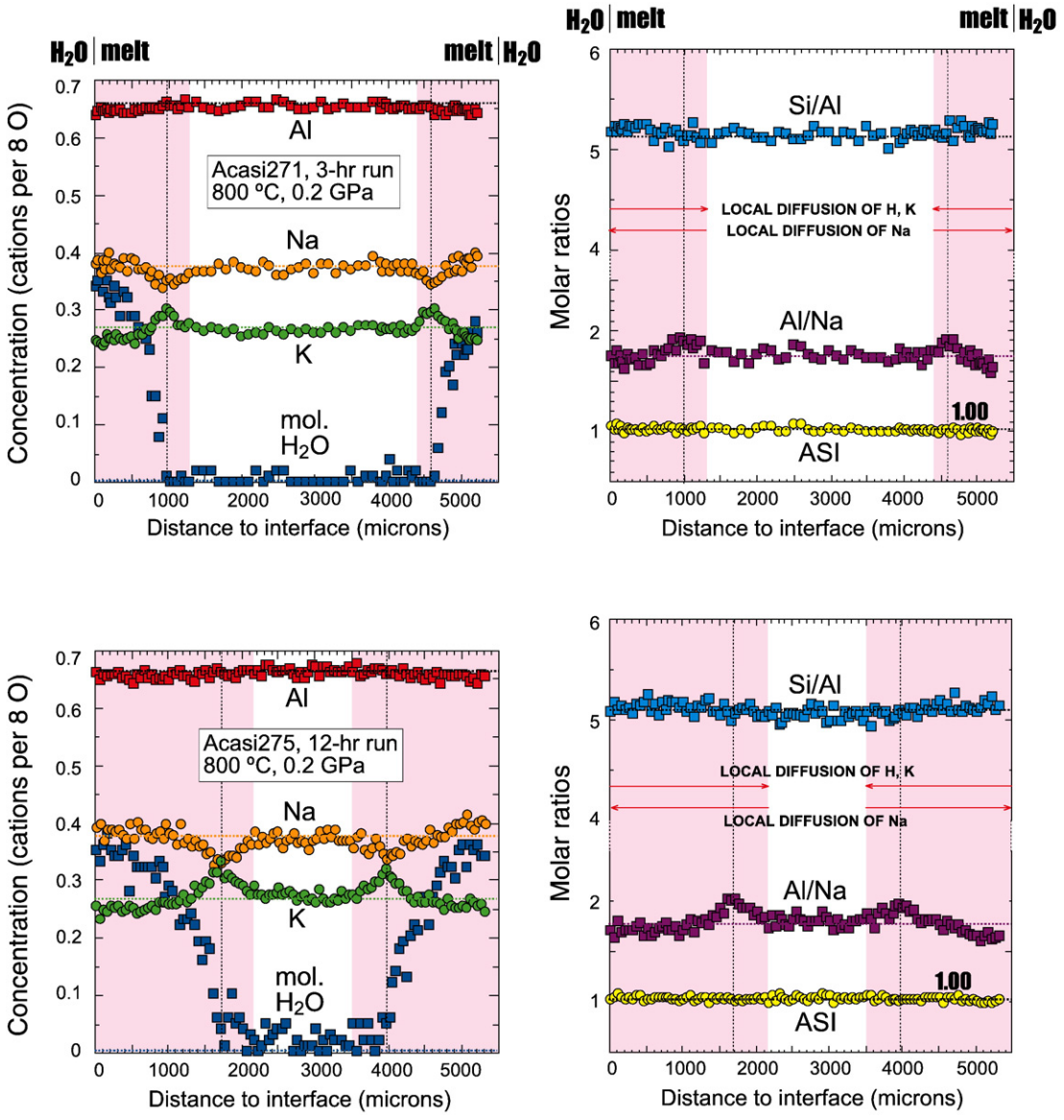

Fig. 10. Composition of glass cores along traverses parallel to their long axes, after the hydration/melting experiments Acasi-271 and Acasi-275, as a function of distance to the H_2O–core interface (see Acosta-Vigil et al., 2005). Dashed vertical lines mark the position of the H diffusion front.

hydration-melting of dry haplogranite glass. The interface melt becomes quickly saturated in H; the H migrates by local diffusion and reaches saturation values progressively away from the interface, in response to the local H concentration gradients produced at the interface during hydration. Concomitantly, Na increases at the interface (with respect to concentrations in the starting glass) and, hence,

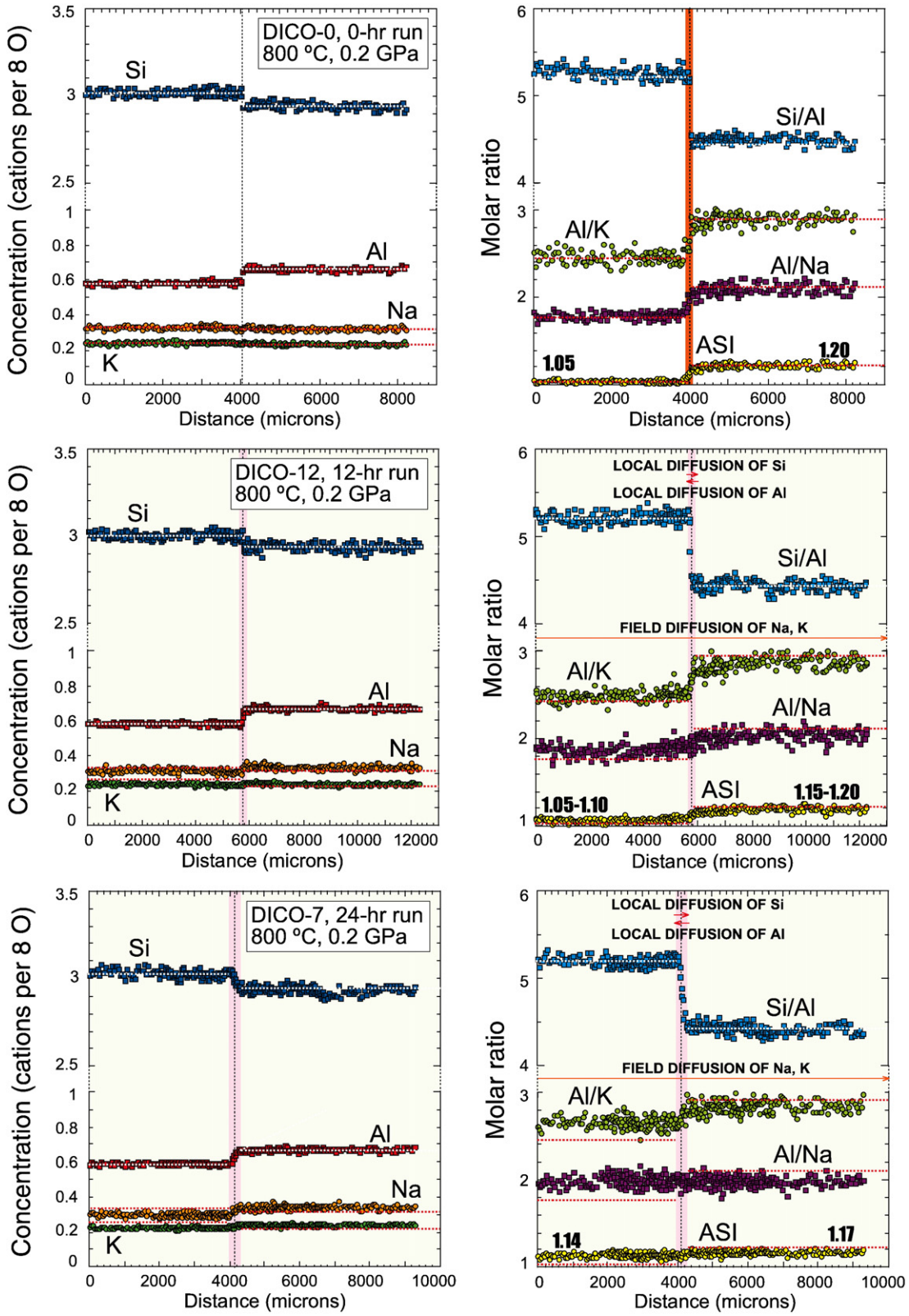

Fig. 11. Concentration profiles in glass after the diffusion couple experiments DICO-0, DICO-7 and DICO-12, across traverses perpendicular to the interface (left panels for element concentrations, right panels for atomic ratios; see Morgan et al., 2008). These experiments juxtaposed metaluminous and peraluminous H_2O-saturated haplogranite melts. The diffusion of alkalis already started in the 0-h experiment DICO-0, as shown by changes in Al/alkalis atomic ratios in the dark orange area. See text for explanation.

diffuses against its own concentration gradient towards the hydrated domain in order to couple with H entering the melt. Simultaneously, there is also a decrease in the concentration of K in the hydrated domain, which diffuses uphill and away from the hydration volume. In this case, the migration of alkalis takes place by local diffusion in response to local concentration gradients of H; this is shown by alkali concentrations at the center of the glass cylinder in the short time experiments (where H has not arrived), which are similar to those in the starting material. In addition, the diffusion of Na and K is such that the ASI of melt stays constant at all times throughout the diffusion volume, i.e. each atom of K leaving the hydration zone is replaced by one atom of Na entering the hydration volume. Note, however, that in this case molar Al/Na is not maintained constant throughout the melt reservoir, as in the case of diffusion along the Al-eigenvector. Aluminum and Si are not involved in the H-eigenvector, as indicated by constant Si/Al ratios throughout the entire melt, similar to those in the starting haplogranitic glass.

3.2.5. Sodium, potassium and field diffusion

From the previous results it is clear that Na and K are strongly coupled with (i.e. assist) the diffusion of Al and H, and that they can diffuse as fast as any other component in the system. The experimental diffusion program reviewed in this contribution has always produced alkali migration in response to diffusion coupling with Al and H, i.e. in response to concentration gradients of Al and H in the melt, and not to concentration gradients in K and Na. However, results suggest that Na and K may represent two other directions of uncoupled diffusion (Na-, K-eigenvectors) in haplogranitic melt, with diffusivities similar to, or higher than, $\approx 10^{-8}$–10^{-9} m^2/s (Acosta-Vigil et al., 2006b, 2012a; Morgan et al., 2008).

To gain information on the diffusivities of alkalis in haplogranitic melt, Morgan et al. (2008) conducted diffusion experiments using diffusion couples where they established an instantaneous and long-range (extending across the entire melt reservoir or couple, ≈1 cm in length) driving force for the diffusion of Na and K. Thus, based on previous results (see above), they juxtaposed two haplogranitic melts with similar composition [concentrations of Na, K, and #K values; #K = mol. $(K_2O / (K_2O + Na_2O)]$ except for the concentration of Al and hence ASI (and Si), entailing an instantaneous Al concentration profile from the very beginning of the experiment (Fig. 11; see also Figs. 2, 3 of Morgan et al., 2008). Experiments lasted from 0 h to six days; during this time frame, Si and Al effectively did not diffuse due to their low diffusivities ($\approx 10^{-15}$–10^{-14} m^2/s) and very short experimental times, except for the longest duration runs where they migrated (by local diffusion) up to ≈100 μm in the vicinity of the interface (Fig. 11; Si and Al concentrations and Al/Si molar ratio are similar to those in the starting glasses). Conversely, alkalis diffused extremely quickly. For instance, during the 0-h experiment — the couple was heated up to the target *T* and, right after this *T* was reached, quickly quenched; this took about 30 min, see Fig. 1 of Morgan et al., 2008 — some diffusion of alkalis had already taken place, as shown by Al/Na, Al/K and ASI profiles at the interface (Fig. 11).

As in the Crn dissolution experiments (Figs. 7, 9), alkalis diffused rapidly via field diffusion throughout the entire length of the melt reservoir, as shown by noticeable changes in ASI, Al/Na and Al/K at the far ends of the couple (with respect to values in the starting materials) in the 6-h run. After 24 h, the Al/Na ratio and ASI are nominally constant throughout the entire 1 cm-long reservoir. These experiments confirm the results of previous Crn dissolution experiments on the stoichiometry of the Al-eigenvector (with an Al/Na ratio similar to that of bulk melt, and ASI equal to that of melt at equilibrium) and, at the same time, provide two insights. (i) The diffusion of alkalis is not instantaneous (at least regarding experimental time frames) as suggested by previous experiments: although it happens at very fast rates, it takes a few hours to erase the Al/Na molar ratio throughout the entire melt. (ii) When all excess Al at the corresponding *P–T–X* conditions is entirely dissolved in the melt (as opposed to being progressively incorporated e.g. during dissolution of Crn into a Crn-undersaturated melt), the diffusion properties of wet haplogranitic melts — and in particular the stoichiometry of the Al-diffusing species — are such that the ASI of the melt is instantaneously homogenized (at geologic and nearly experimental time frames) throughout the entire interconnected melt reservoir, as in the case of the Al/Na molar ratio (Fig. 11; and Fig. 3 of Morgan et al., 2008). We stress that these observations regarding the redistribution of alkalis (as well as the rest of melt components described in previous experiments), are based on time series experiments were diffusion was the only mass transport mechanism in the melt. That is, flow of melt did not occur as shown, among other things, by the regular concentrations profiles obtained in all the experiments (see for more details Acosta-Vigil et al., 2002, 2006a, 2006b; Morgan et al., 2008).

The stoichiometry of the Al-diffusing component, combined with the mechanism of field diffusion for alkalis, have at least two direct

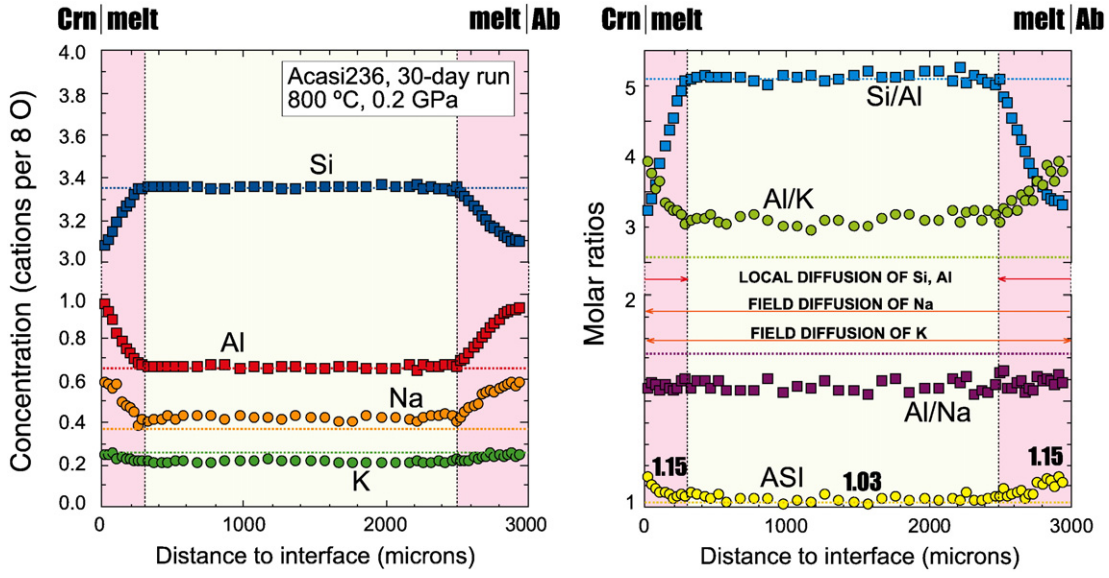

Fig. 12. Composition of glass after the "sandwich" dissolution experiment Acasi-236, as a function of distance to one of the mineral–melt interfaces (see Acosta-Vigil et al., 2006b). In this experiment, H_2O-saturated metaluminous haplogranitic melt was placed in between corundum, to the left, and albite, to the right. See text for explanation.

applications in studies of crustal anatexis. (1) These diffusion systematics imply that physically interconnected melt in a migmatite can change its composition simultaneously and instantaneously, independently of the size of the interconnected melt reservoir. As an example, see in Fig. 12 how the ASI of a metaluminous (ASI ≈ 1.0) melt increases at the interface with a diffusively dissolving Ab, during an Ab–melt–Crn sandwich dissolution experiment, before any of the slow-diffusing Al coming from the diffusive dissolution of Crn has arrived at the Ab–melt interface (see also Figs. 4, 12 of Acosta-Vigil et al., 2006b). This is because, although Ab has an ASI ≈ 1.0, Crn is dissolving into the metaluminous melt at the other end of the reservoir, progressively increasing the melt ASI at the Crn–melt interface up to the equilibrium value with Crn at those *P*–*T*–*X* conditions (ASI ≈ 1.20, Acosta-Vigil et al., 2003). This causes the ASI of the Al-diffusing species migrating through the melt to homogenize Al, e.g. away from the dissolving Ab, to be ≈1.20, and hence produces an instantaneous increase in ASI at the Ab–melt interface from the very onset of Ab dissolution. For comparison, when a single crystal of Ab dissolves into a metaluminous melt at similar *P*–*T*–*X*-time conditions, the interface melt has an ASI ≈ 1.0, which is the equilibrium ASI of melt under those *P*–*T*–*X* values (see Fig. 5 of Acosta-Vigil et al., 2006b). (2) The Al/Na and ASI molar ratios constitute proxies for melt interconnection because, if the following two conditions hold, they will become instantaneously constant throughout a melt reservoir. (i) Al concentration gradients must be present in the melt, in order to trigger Al diffusion and the coupled diffusion of Na to produce constant Al/Na ratios. In most cases it seems reasonable that Al gradients will exist in the melt, e.g. Al increasing towards dissolving feldspars and/or peraluminous minerals, and/or decreasing towards Qtz. (ii) All excess Al in melt at equilibrium with the residue must be rapidly transferred into the melt during the melting reaction, as opposed to being slowly incorporated by dissolution of the residual peraluminous minerals, e.g. Ms, Bt or Sil (see the constant ASI throughout the entire melt reservoir after only 24 h, Fig. 11); this second condition might be more difficult to meet.

4. Limitations on the applicability of the experimental observations to natural scenarios

Transferring experimental observations to the study of processes in Nature is not trivial. Below we discuss how variations in the conditions of the system (pressure, activity of H_2O and presence of differential stress), spatial scale (size and nature of the starting material) and, most importantly, time scale of anatexis (directly related to the rate of heat supply), affect the previous observations and conclusions and their application to natural scenarios.

4.1. Melting conditions: pressure, activity of H_2O in melt and presence of differential stress

Pressure seems to have a small influence on the diffusivities of components in granitic melts: Baker (1990) showed that diffusivities in dacitic and rhyolitic melts increase by a factor of 4 going from atmospheric pressure to 1.0 GPa (at 1300 °C). Hence previously calculated time frames, based on diffusivities at 0.2 GPa H_2O, can reasonably apply to anatexis in the middle and lower continental crust as well.

The activity of H_2O has a strong influence on melt diffusivities, as they vary by one order of magnitude for every ≈3 wt% H_2O in the melt (Baker, 1991; Watson and Baker, 1991). Slower diffusivities associated with a decrease of a_{H2O} in melt imply longer time frames for melting (in the case of diffusion in melt-controlled melting) and melt homogenization, and this effect needs to be assessed by investigating diffusivities in melt and kinetics of melting at low H_2O activities. Hence our estimations of melt homogenization timeframes (Fig. 6) represent minimum values; considering H_2O concentrations of ≈3 wt% in crustal melts generated by H_2O-absent hydrate-breakdown anatexis in the middle and lower continental crust (e.g. Holtz et al., 2001), the above time frames would increase by approximately one order of magnitude. In addition, recent studies have shown that regional anatexis under H_2O-present conditions might be much more frequent than previously thought (Carvalho et al., 2016; Sawyer, 2010; Weinberg and Hasalová, 2015; and references therein); in these cases, the above time frames based on diffusivities in H_2O-saturated melts could be directly applicable (for the particular cases of H_2O-saturated melting).

Saturation in H_2O may also have an effect on melt distribution, as H_2O may migrate along grain boundaries throughout the rock, transport granite components such as alkalis, and produce melting where the local assemblage is not eutectic, e.g. along Pl–Kfs, Qtz–Qtz boundaries. In this regard, Brearley and Rubie (1990) partially melted muscovite schist cylinders both under H_2O-saturated and H_2O-undersaturated (no added H_2O) conditions, and found in both cases that melt formed narrow rims in between reactants throughout the entire cores from the beginning of melting, apparently constituting a grain boundary network. In addition, H_2O-absent partial melting experiments of pelites indicate that, even under hydrostatic conditions, muscovite melting reactions can create a transient permeability and interconnection of the melt phase that may promote melt segregation (Rushmer, 2001). These observations suggest that excess H_2O does not have any influence on melt distributions during the experimental melting of rock cylinders, though this matter needs further investigation.

Field and experimental studies have shown that partial melting under differential stress produces a tendency for melt to temporarily wet grain boundaries and achieve melt interconnection (Holness, 2010; Holyoke and Rushmer, 2002; Jin et al., 1994; Rosenberg and Riller, 2000; Rushmer, 1995; Rutter and Neumann, 1995; Sawyer, 2001). Mechanical mixing during deformation and melt segregation/extraction, on the other hand, decreases melting and homogenization times, particularly when melting is diffusion-controlled, because it "refreshes" the melt composition in contact with dissolving minerals (increasing the rate of melting) and increases the chemical homogeneity of melt (e.g. Watson, 1982). This phenomenon, though, is difficult to quantify and is beyond the scope of this work.

4.2. Spatial scale: size and nature of the starting material

The experimental program reviewed in this article was designed to explore the kinetics of melting/dissolving crustal minerals and systematics of diffusion in granite melts, by progressively increasing the complexity of the experimental design, going from single-mineral dissolution experiments and glass hydration/melting experiments, to two-mineral (sandwich) dissolution experiments, to the melting of natural rock cores. The latter experiments showed the same systematics of diffusion in granite melt found in the simpler mineral dissolution experiments. Most importantly, they replicate anatexis in nature much more closely than other experiments where the starting materials are fine-grained mineral mixtures. This is because the composition, grain shape and size, and mineral distributions and microstructural relationships in the starting material are exactly those of a crustal protolith. Thus, the melt distribution observed in the experiments can be scaled up to natural rocks without extrapolation, because of the large size of the rock cylinder with respect to the average mineral grain size.

4.3. Time scale: rate of heating-limited crustal anatexis

Observations on the controls on, and time frames of, melting, melt composition, melt homogenization and melt–residue equilibration described above (Section 3) apply to examples of anatexis where the heat supply is transiently infinite, such as to overstep the melting reaction to a certain degree — i.e. to rapidly impose and temporarily maintain *T* at a value above that of the equilibrium melting *T* (at a given *P*). This applies directly to contact anatectic settings, associated e.g. with the intrusion of mantle magmas (e.g. Holness et al., 2005). The latter, however, might be an uncommon scenario for the generation of

voluminous granitic magmas in the continental crust, which has been traditionally thought to be associated with regional anatexis under H_2O-undersaturated conditions, via H_2O-absent hydrate-breakdown melting reactions (Clemens and Watkins, 2001; Stevens and Clemens, 1993); these conditions seem to be typical of continental collision settings. However, there are at least two important tectonic/geologic settings regarding the generation and differentiation of continental crust, where regional anatexis associated with a transiently infinite supply of heat can definitely occur, and hence the above conclusions are applicable: (i) in subduction and rifting scenarios during the intraplating of mantle magmas (Annen and Sparks, 2002; Annen et al., 2006; Dufek and Bergantz, 2005); and (ii) during the rapid influx of H_2O-rich fluids in rocks that were already well above their wet solidus, such as major regional-scale shear zones (Brown, 2010; Carvalho et al., 2016; Sawyer, 2010; Weinberg and Hasalová, 2015).

During regional anatexis in collisional settings via H_2O-absent hydrate-breakdown melting reactions, the rate of heat supply is much slower than in contact anatectic settings, and heat supply is considered to be the rate-limiting process in the generation of melt; the rate of melt generation will be ultimately controlled by the interplay between the rate of heating, the heat capacity and thermal diffusivity of rocks, and the latent heat of melting (e.g. Brown, 2010; Harris et al., 2000; Rubie and Brearley, 1990). Calculations indicate that, in cases where the heat consumption during endothermic melting reactions buffer *T* at the equilibrium melting temperature, generation of significant proportions of melt fractions may require hundreds of thousands of years or even several millions years (De Yoreo et al., 1989; Hodges et al., 1988; Rubie and Brearley, 1990; Stüwe, 1995). Hence, a common view is that the approach to the solidus and melting in these regional settings occurs at exceedingly slow rates, at or close to equilibrium. To date, however, there are no estimates of the time scales required to achieve textural equilibration during anatexis (Holness, 2010). Also, although migmatites are solidified rocks that have lost the original melt bearing microstructures, detailed studies of regional metamorphic migmatites find disequilibrium, reaction-controlled melt distribution (Holness and Sawyer, 2008) and, in general, textural disequilibrium seems to be the rule rather than the exception (Holness, 2010). In addition, case studies on the geochemistry of regional migmatites in collisional orogens frequently describe disequilibrium melting regarding trace element concentrations in melt, associated with rapid melt segregation (e.g. Barbero et al., 1995; Barbey et al., 1989; Bea, 1991; Watt and Harley, 1993). This, in turn, indicates rapid melting and melt interconnection. Hence, (i) slow rates of heating in collisional settings do not necessarily imply that anatexis proceeds at slow rates and under textural and/or chemical equilibrium, and (ii) the nature of melt distribution, and controls on melting rate, melt composition and extent of melt–residue equilibrium in this environment are not clear and further detailed studies are required. Current studies on migmatites (see above), nevertheless, suggest that these characteristics might approach those described during the granite core melting experiments, particularly at low degrees of overstepping, i.e. rapid melt interconnection, disequilibrium melt distributions and compositions, lack of residue recrystallization, and long time frames for melt–residue equilibration.

Some experimental studies and numerical modeling by Rubie and Brearley (1990) and Rubie (1998) indicate that, even in cases of regional anatexis where overall the rate of heat supply constitutes the rate-limiting process, there can be an initial period where, due to the kinetics of melting (e.g. the sluggish nucleation of products during peritectic melting reactions), a large *T* overstep is possible. And, associated with this overstepping, a large amount of melt can be produced in a very short time interval, during which the rate of melting is controlled by the kinetics of the melting process (interface reactions, diffusivities in melt). For instance, these authors calculated that an overstep of 20–100 °C would produce 20–50% of melt in 0.2–1 year. In these situations, melting rates, melt compositions and time frames for melt homogenization and melt–residue equilibration can be similar to those described during experimental melting at different degrees of overstepping, e.g. at high degrees of overstepping we should expect rapid melt interconnection, initially heterogeneous disequilibrium compositions, extensive recrystallization of residue, and short time frames for melt–residue equilibration.

Comparison of the above experimental results (Section 3) with the analyzed compositions of primary melts in natural scenarios — and in particular, of MI — as well as with compositions and homogeneity of residual minerals — for example, Pl — may provide clues to the nature and mechanisms of anatexis in natural environments. This is discussed in the next section.

5. Nature of primary melt compositions during crustal anatexis

5.1. How do we obtain the composition of primary anatectic melt?

The field, petrological and geochemical analysis of migmatites provides a first, necessary and important approach to the study of primary crustal melt compositions, particularly when systematic geochemical investigations are conducted throughout the anatectic terrane, in order to understand the processes active during partial melting (e.g. Carvalho et al., 2016; Sawyer, 1998, 1999). However, leucosomes may not provide precise information on primary melt compositions, because (i) they are thought to constitute parts of a macroscopic network along which melt is either drained from the studied terrane, and/or transferred from deeper to upper crustal levels (e.g. Brown, 2013; Sawyer, 2001); and (ii) primary melts are commonly affected by/associated with phenomena such as entrainment of residue and, upon cooling, fractional crystallization and separation of melt from minerals, interaction with the residue and crystallization with H_2O loss (e.g. Brown, 2013; Carvalho et al., 2016; Sawyer, 1999, 2008; White and Powell, 2010).

To obtain further information on primary melt compositions and processes during anatexis, leucosome compositions are commonly compared with experimental glass compositions produced during partial melting of crustal protoliths at *P–T–X* conditions similar or close to those inferred for the anatectic terrane (e.g. Carvalho et al., 2016; Morfin et al., 2014; Solar and Brown, 2001). Although it provides a wealth of information, this approximation may also have some drawbacks: (i) there may be differences in bulk rock composition and *P–T* of melting between studied and experimentally melted rocks (Bartoli et al., 2013c; Cesare et al., 2015); and (ii) this approach commonly ignores the kinetics of crustal melting. For instance, starting materials in the experimental studies are commonly powdered rocks, and experimental glass is thought to represent the composition of melt at equilibrium with the residue at the investigated *P–T* conditions. However, compositional zonation in major minerals of anatectic terranes controlling both major and trace element compositions of melts (e.g. Pl, Grt) is ubiquitous. In fact, many geochemical studies in anatectic terranes have found that, based on the trace element concentrations of leucosomes, melts were not at equilibrium with their residue (e.g. Barbero et al., 1995; Barbey et al., 1989; Bea, 1991; Sawyer, 1991; Watt and Harley, 1993; Watt et al., 1996). In addition, and based on kinetic considerations, Bea (1996) concluded that chemical equilibrium during anatexis is the exception rather than the rule, at least regarding the distribution of trace elements between melt and residue. Hence, why should we assume mineral–melt major element equilibrium distributions during anatexis?

Some of the drawbacks regarding the study of the compositions of primary crustal melts, through the approximations of leucosomes in anatectic terranes and glasses in experimental studies, can be overcome with the study of MI. Two decades ago, primary MI were discovered in crustal anatectic rocks, first in enclaves within peraluminous dacites — where MI have solidified to glass upon rapid ascent and extrusion — (Cesare et al., 1997), and later on in crustal anatectic terranes — where MI commonly crystallize to a granitoid assemblage with grain

size ≤1 μm, and hence have been termed nanogranites or nanogranitoids — (Cesare et al., 2009, 2015). Their mode of entrapment guarantees that these MI represent primary anatectic melts present in the rock during growth of their host peritectic minerals (Bartoli et al., 2014; Cesare et al., 2011, 2015). In addition, recent studies have shown that MI are commonly present in anatectic terranes (Bartoli et al., 2016a; Cesare et al., 2009, 2011, 2015; Ferrero et al., 2012). Primary melt inclusions have also been described in UHP gneisses and eclogites associated with the subduction of continental crust (Frezzotti and Ferrando, 2015; Hwang et al., 2001; Korsakov and Hermann, 2006; Stöckhert et al., 2001; and references therein), where they have been called melt inclusions, multiphase inclusions or polyphase inclusions, and have been interpreted as former melt or dense supercritical fluids.

This new approach, however, may also involve some potential weaknesses that need to be explored. Even though Bartoli et al. (2013b; see also references therein) have developed an appropriate methodology to rehomogenize nanogranitoids in order to extract their precise composition, there is still uncertainty over how representative MI are of the bulk melt present in the rock at the time of entrapment. This, in turn, translates into uncertainty about the meaning of their compositions, or what kind of information they provide about anatectic processes (see also Cesare et al., 2015). These doubts are due to at least two reasons. One is associated with the fact that the analysis of MI in anatectic rocks represents a new approach to the study of anatexis that is currently being developed, as more MI analyses from different anatectic terranes worldwide become available a clearer picture will emerge (Bartoli et al., 2016a; Cesare et al., 2015). The other is directly related to the lack of abundant and/or fully described information in the literature on how primary crustal anatectic melts are established, and what are the main factors governing their compositions. This article is intended to fill this gap and **provide a reference frame** (Sections 2 to 4) from the melting experiments to which the composition of MI can be compared in order to extract the information that MI contain on the process of anatexis. After some consideration on the meaning of MI compositions (Section 5.2), we test this reference frame with the currently published compositional information of glassy MI from the El Hoyazo anatectic enclaves (Section 5.3) and nanogranitoids in regional migmatites and granulites around the world (Section 5.4).

5.2. Interpretation of the compositions of melt inclusions

Cesare et al. (2011, 2015) and Bartoli et al. (2014) have shown that, because MI in anatectic rocks are trapped within peritectic minerals formed concomitantly with the melt, their compositions must correspond to those of primary anatectic melts, i.e. those produced during the anatexis of the rock. In addition, this mode of generation entails that MI should likely record melts produced in situ, as opposed to melts flowing along grain boundaries; that is why comparing their compositions with the reference frame laid out above (Sections 2–4) may provide information on the controls on primary melt compositions before segregation. Some of the retrieved characteristics may represent **minimum** values (e.g. degree of melt homogeneity or melt–residue equilibration), as once MI are trapped they will not likely interact any more with the rock matrix (see Bartoli et al., 2014). Nevertheless, what is the precise meaning of the composition of MI, and what are they telling us about the melting process? There are two extreme scenarios. On the one hand, they may represent (i) a homogeneous melt present in the migmatite at the time of entrapment. On the other hand they may record (ii) a melt that is heterogeneous for different reasons; one of these is that they might record melts produced at different times along the prograde path or during different anatectic events (e.g. Acosta-Vigil et al., 2010, 2016; Bartoli et al., 2015). And this is the basis for MI representing a window of information into the (prograde or polyphase) anatectic history of a migmatite (Acosta-Vigil et al., 2010, 2016). Hence, when studying MI compositions it is important to couple compositional and microstructural observations, i.e. we must specify in what mineral or mineral domain the analyzed MI is present, and to which mineral association/assemblage in the rock does this microstructural domain belong (Cesare et al., 2011, 2015; Ferrero et al., 2012).

If MI compositions are homogeneous, then they may represent (i.a) melt at equilibrium with the residue, either the bulk residue (case i.a1: coexisting minerals are homogeneous and show major and trace element equilibrium partitioning with respect to the MI), or just with the rims of minerals (case i.a2: coexisting minerals are heterogeneous and show equilibrium partitioning distributions only at the contact with MI); or (i.b) a homogeneous disequilibrium melt, where melting is controlled by the kinetics of the interface reactions (see Section 3.1.1).

When the composition of MI found within a mineral or minerals pertaining to a single assemblage in the rock (i.e. MI formed at the same time) are heterogeneous, there are essentially three possible interpretations. (ii.a) MI compositions are locally controlled by the kinetics and interplay of processes acting in the vicinity of mineral host–melt interfaces, which include boundary layer phenomena and enrichment of elements in the surface layer of rapidly growing crystals (e.g. Albarede and Bottinga, 1972; Baker, 2008; Watson, 1996). In this case their applicability to the study of crustal anatexis might be limited, as fractionation among major and trace elements at the interface melt region — controlled by the interplay between mineral growth, melt diffusivities, element compatibility with the growing mineral and disequilibrium mineral–melt partitioning — could modify to a large extent the composition of the bulk melt present in the migmatite. The few currently available studies have concluded that the kinetics of processes acting at interfaces do not modify the original major element and incompatible (with respect to the mineral hosts) trace element concentrations of melt trapped as MI in migmatites; they may influence, however, the concentrations of the compatible trace elements, that may show disequilibrium distributions and enrichment in the surface layer of the rapidly growing host (Acosta-Vigil et al., 2010, 2012b; Bartoli et al., 2016a; Cesare et al., 2015). This issue is important and requires further and detailed examination as more case studies of MI become available. (ii.b) Even if during entrapment MI were recording matrix melt compositions unaffected by processes acting at interfaces, they would be modified later by post-entrapment processes, such as dissolution or crystallization of the host, crystallization of daughter minerals, and H_2O loss (e.g. Roedder, 1984). This will again limit the applicability of MI to the study of crustal anatexis, though currently available studies suggest that these processes do not significantly affect MI compositions in migmatites (Cesare et al., 2015). These two first possibilities can be examined using the geochemical procedures described in the extensive studies of MI present in phenocrysts of volcanic rocks (e.g. Audetat and Lowenstern, 2013; Kent, 2008; Roedder, 1984; and references therein). (ii.c) MI may document melts whose compositions are locally controlled by the nature of neighboring reactants contributing to the melt ± residual minerals (e.g. Clemens, 2009); these melts, however, are **representative of those particular domains** of the rock (see Section 3.1.2). In addition, if melt is interconnected and if the time interval between generation and entrapment allows, these local compositions will necessarily evolve with time towards a homogeneous melt, according to the systematics of diffusion in melt (Section 3.2), ending in cases (i.a1), (i.a2) or (i.b) as a function of the extent of melt–residue equilibration.

All scenarios except (ii.a) and (ii.b), are exactly equivalent to those simulated in the kinetics experiments described above that explore the processes that control the mechanisms and timing of anatexis (Section 3). In these cases, melt composition at a given time and location in the rock is determined by the interplay between the kinetics of the interface reactions, the kinetics and systematics of diffusion in melt and minerals, the possibility of mineral recrystallization, and the time available between melt generation and MI entrapment (Fig. 4). In these scenarios (i.e. once we are sure that MI compositions do not correspond to cases ii.a or ii.b), therefore, the study of MI and coexisting minerals, and comparison with experimental results from kinetics and equilibrium

studies on anatexis, constitutes a tremendously useful tool to investigate the partial melting of the continental crust.

From the above it is clear that MI can provide information not only on the compositions of primary melts (i.e. those produced during the process of partial melting; Bartoli et al., 2014; Cesare et al., 2011, 2015), but also on the nature and mechanisms of anatexis in a particular rock and geodynamic setting. This includes the extent to which melt was homogeneous, interconnected and at equilibrium with the residue before entrapment, and hence information on the roles of diffusion in melt, interface reaction and mineral recrystallization during melting and, possibly, on the occurrence/extent of overstepping. Melt inclusions also provide information on the nature of melting reactions and fluid regimes (see Acosta-Vigil et al., 2010, 2012b; Bartoli et al., 2014; Cesare et al., 2015). All this information can be gained by comparing MI and coexisting mineral compositions gathered from a particular migmatite, with published data both on the equilibrium melting and melting kinetics of systems that are (closely) similar in composition to the investigated rock. This includes major element equilibrium melt compositions (e.g. eutectics), mineral–melt trace element equilibrium distribution coefficients, accessory mineral saturation concentrations of trace elements in melt (e.g. Zr and LREE concentrations in Zrn and Mnz saturated melts, respectively), and information on mechanisms and kinetics of melting such as that shown in Section 3 (e.g. role/interaction of processes occurring during anatexis, and systematics of diffusion in melt).

From the previous discussion it is clear also, and **we stress** that, if MI compositions are not homogeneous and/or at equilibrium with the residue, this does not mean either that MI are not recording primary melts, or that they are not representative of the melt present in the migmatite during entrapment, or that they provide just local, unrepresentative and useless information. It only means that they record the anatectic environments where they form, and processes happening in a particular part of the migmatite during anatexis, as leucosome compositions may record anatexis at disequilibrium, or fractional crystallization of melt upon cooling.

Kinetics data are quite important, as for instance during diffusion-controlled melting, the nature of the progressive homogenization among local melts within the minimum volume for equilibrium depends on the systematics of diffusion. Thus, considering only diffusivities, one would expect fast-diffusing components — e.g. Na, K, H — to homogenize concentrations in melt much faster than slow-diffusing components — e.g. Si, Al. However, this is not true when fast diffusing components are coupled with the diffusion of slow diffusing components, as in the strong coupling of Na and K with Al through the Al-eigenvector. In this case, concentration gradients of alkalis in melt may be present and persist until those in Al are erased through diffusion along the Al-eigenvector. Also, and regarding directions of uncoupled diffusion, Al/Na ratios, or even ASI under certain circumstances (see above), are expected to homogenize almost instantaneously throughout all interconnected melt, whereas Si and Al concentrations and Al/Si molar ratios will take a long time to do so. That is why Al/Na and ASI ratios can potentially be used as proxies for melt interconnectivity. Fig. 13 schematically illustrates scenario (ii.c) during the particular case of H_2O-absent Bt-dehydration melting, and provides expected concentration profiles in the melt in between residual and peritectic minerals, based on the previously described diffusion systematics of granite melts.

In order to interpret the significance of MI compositions analyzed in a particular anatectic rock, one should ideally obtain the following information. (i) As in any other geochemical study, a relatively large number of high quality and microstructurally controlled MI analyses. (ii) When MI are only present within a single mineral of a single-protolith migmatite, analyze MI within several crystals of that mineral in a few thin sections made from different rock chips/hand specimens of the outcrop; this will help evaluating the degree of melt homogeneity at the mm–cm–dm scale and contrast results with the estimated minimum volume for equilibrium. (iii) When MI are present within several minerals pertaining to different mineral assemblages, or in different microstructural locations of a single mineral grown during the suprasolidus evolution of the rock (e.g. Grt cores versus Grt rims), then investigation of MI compositions throughout these different microstructural locations — if abundance, preservation and size of MI allow — may provide information on the (prograde, polyphase) anatectic history of the rock. (iv) When matrix melt (glass) is present, such as in enclaves of regional anatectic migmatites within lavas, analyses of matrix glass may help determine the extent to which syn- and post-entrapment processes (e.g. boundary layer phenomena) control the compositions of MI. (v) In the case of migmatites formed from heterogeneous protoliths, analysis of MI within minerals of the several protoliths, if available, may provide some information on the (maximum?) extent of melt heterogeneity expected to be inherited from the source region, in addition to that associated with the incomplete homogenization of melt formed from single-protolith migmatites due to sluggish diffusion; this information can be compared with results from studies of intrusive granitoids proposing

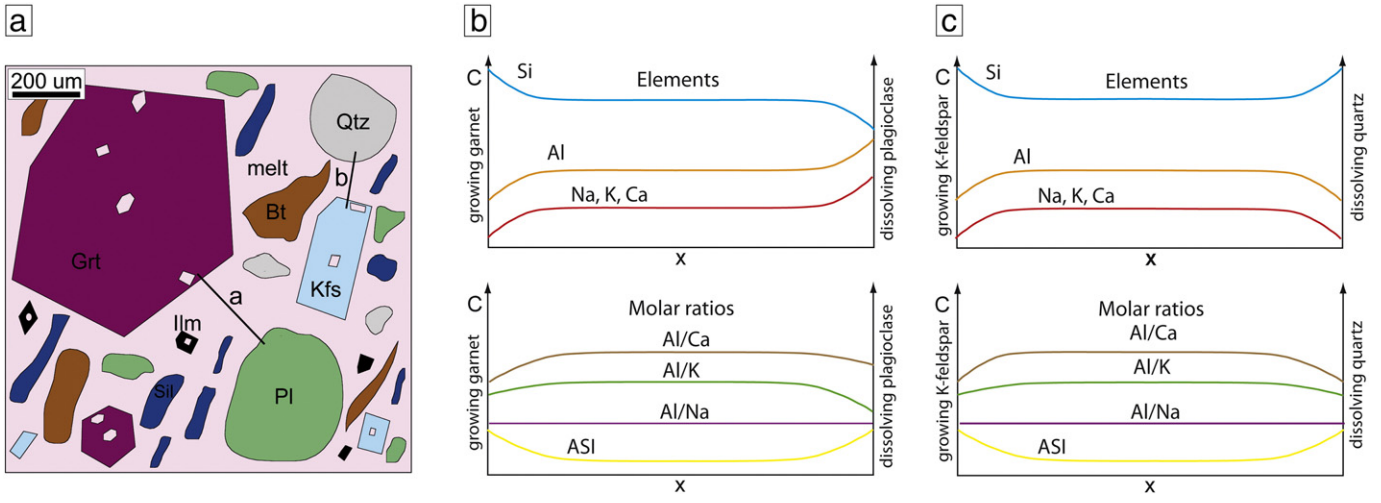

Fig. 13. (a) Schematic two-dimensional section of the minimum volume for equilibrium in metasedimentary rock undergoing partial melting by the peritectic reaction Bt + Sil + Pl + Qtz = Grt + Kfs + melt + Ilm. (b) and (c) show schematic concentrations profiles in melt between peritectic Grt and residual Pl, or between peritectic Kfs and residual Qtz, respectively, during diffusion-controlled melting of the rock, and before total melt homogenization has taken place. Notice unexpected increases of ASI towards dissolving Pl and Qtz, K towards dissolving Pl, or constant Al/Na molar ratios. See Section 3 for further explanation.

this process as important in shaping bulk rock geochemistry (e.g. Clemens and Benn, 2010). (vi) Major and trace element compositions of minerals coexisting with the MI (both hosting MI and MI-free minerals) should be obtained in order to evaluate the extent of melt–residue equilibration during anatexis (see also Acosta-Vigil et al., 2010, 2012b, 2016).

5.3. Information from MI in anatectic enclaves: the example of El Hoyazo

Strongly peraluminous, ≈6 Ma old post-orogenic dacites of El Hoyazo (Betic Cordillera, S Spain) are crowded with foliated metasedimentary anatectic enclaves that have residual compositions, suggesting loss of ≈30–60 wt% of a granite melt component. The enclaves still have ≈10 wt% of melt present as abundant primary MI within most of the minerals (Pl, Grt, Bt, Crd, Kfs, Ilm, Spl, Ap, Mnz, Zrn) and in the matrix as films of glass along foliation planes and surrounding minerals. Melt was produced mostly in a regional setting before incorporation within the magma, and solidified to glass due to rapid cooling upon ascent and extrusion. This is inferred from microstructures documenting syn-anatectic deformation, presence of MI-bearing minerals wrapped by the main foliation, and the residual nature of enclaves indicating melt loss. These observations are difficult to explain if melting was after incorporation in the magma. These enclaves, therefore, represent a snapshot of anatexis in the middle-to-lower continental crust (see below), frozen due to ascent and extrusion within the dacite, where melt and residue can be readily identified and analyzed (Acosta-Vigil et al., 2010; Cesare and Gómez-Pugnaire, 2001; Cesare et al., 1997, 2015; Zeck, 1992; Zeck and Williams, 2002).

Cesare and Maineri (1999) noticed that MI are present within both reactants and products of typical melting reactions in metasedimentary protoliths. They hypothesized that this is due to the (re-)crystallization of all minerals in the presence of melt, during the process of rapid disequilibrium melting of a low-grade phyllite, which equilibrated mineralogically to granulite facies conditions, possibly by-passing most amphibolite facies reactions. They proposed the following melting reaction:

$$\mathrm{Chl} + \mathrm{Ms} + \mathrm{Qtz}\ \mathrm{Ilm} + \mathrm{GCOH\ fluid}\ (\pm\mathrm{St} \pm \mathrm{Kfs} \pm \mathrm{Ky}) = \mathrm{Grt} + \mathrm{Pl} + \mathrm{Sil} + \mathrm{Bt} + \mathrm{melt} + \mathrm{Gr},$$

where "GCOH fluid" stands for a mixture of H_2O, CO_2, CH_4, CO and H_2, and noticed that the reaction products appear equilibrated from a mineralogical and compositional point of view. The term "disequilibrium melting" was likely used to stress the presence of the original reactant assemblage (low-grade phyllite) outside its stability field, and the overstepping of most intermediate reactions between the low-grade phyllite and the granulite-facies migmatite.

Plagioclase, Grt, Bt, Sil and melt have been included within the main equilibrium assemblage of the enclaves, for which thermobarometric calculations using Grt–Bt and Grt–Pl pairs obtained conditions of ≈ 800–850 °C and 0.5–0.7 GPa (Cesare and Maineri, 1999; Cesare et al., 1997). Melt in this assemblage corresponds to the matrix glass coexisting with these minerals. Instead, MI located at the cores of Pl and Grt formed before matrix glass and represent matrix melts present in the migmatite during (re-)crystallization of these cores, and therefore constitute the remains of the first melts produced during anatexis of the enclaves that we can have access to.

Previous studies have documented the major and trace element compositions of MI in Pl, MI in Grt and matrix glass, as well as the coexisting minerals, as mean concentrations and normative Qtz–Or–Ab–An, Harker, chondrite-normalized REE and spider diagrams (Acosta-Vigil et al., 2007, 2010, 2012b; Bartoli et al., 2016a; Cesare and Acosta-Vigil, 2011; Cesare et al., 1997, 2011, 2015). Figs. 14 and 15 show the compositions of MI and matrix glass in enclaves as wt% CIPW normative Qtz–Or–Ab and Harker diagrams, and compare it with the glass produced in the granite core melting experiments at low and high degrees of *T* overstepping (Sections 3.1.1 and 3.1.2). Although MI are present in virtually all minerals in the enclaves, ≈250 MI were mostly analyzed at the cores of Pl and Grt, as these minerals show abundant, well-preserved and sufficiently large MI. Analyses come from three petrographically similar (Grt–Bt–Sil) enclaves and several crystals of Pl and Grt in each of them. Matrix glasses were additionally analyzed across the entire thin sections. The relative position of these enclaves in the source area before incorporation into the dacite is uncertain. Given that the dacites constitutes a ≈1-km diameter dome crowded with enclaves, it is likely that analyzed enclaves were originally located at least meters to tens-hundreds of meters apart. Despite this, all MI show systematically peraluminous K-rich leucogranitic compositions similar to glass produced during the H_2O-absent hydrate-breakdown experimental melting of metasediments (SiO_2 = 69–76 wt%, $FeO_t + MgO + TiO_2$ = 0.5–2.5 wt%; #K = 0.40–0.65; ASI = 1.05–1.40, compared with e.g. Vielzeuf and Holloway, 1988). In addition, they plot in the vicinity of (≈0–20 wt%) H_2O-undersaturated haplogranitic eutectics and Qtz–Or cotectic line (Fig. 14). Based on diagrams in Figs. 14 and 15, information on trace element concentrations in the glasses and residual minerals (Acosta-Vigil et al., 2010, 2012b), previous data and the discussion on the kinetics of partial melting (Sections 3–5), we infer below some major features of the process of anatexis of these enclaves.

In the normative Qtz–Or–Ab diagram (Fig. 14), glasses from MI show a larger compositional spread with respect to the mostly homogeneous experimental glasses produced at low degrees of *T* overstepping (690 °C), and plot relatively far from the haplogranite eutectics. Despite this, and considering that analyses come from several enclaves and different Pl and Grt crystal hosts, it is remarkable that glass in each microstructural location is characterized by a distinct composition (Figs. 14, 15). MI in Pl have the most heterogeneous and incompatible element-rich compositions, showing large variations in ASI, Al/Na and #K, and lack of any trend in most diagrams. MI in Grt and the matrix glass show the least geochemically evolved and most homogeneous compositions, in particular matrix glass shows quite constant Al/Na ratios. The still relatively heterogeneous MI in Grt form a clear trend parallel to the Qtz–Ab side line, similar to those of experimental glasses produced at high degrees of *T* overstepping (800 °C), where melting was diffusion in melt-controlled (Fig. 14); this trend is absent from the MI in Pl, and less clear in the relatively homogeneous matrix glass. Assuming that MI major element concentrations were not affected either by pre- or post-entrapment processes (cases ii.a and ii.b, respectively, Section 5.2) (Acosta-Vigil et al., in preparation), the above observations suggest that diffusion in melt controlled the rate of melting during anatexis of the enclaves, and hence that melting was associated with a large *T* overstep of the reaction (case ii.c, Section 5.2; and Section 3.1.2). Also, melt likely had progressively longer time frames for homogenization going from MI in Pl to MI in Grt (i.e. time between melt generation and entrapment) and to matrix glass (time between generation and quenching) (Fig. 14). MI in Pl seem to represent former local matrix melt that either was not interconnected before entrapment, or was rapidly trapped after formation; otherwise their Al/Na ratio would not be that heterogeneous (Fig. 15). The matrix glass and MI in Grt represent melts, likely interconnected, that had more time to homogenize and given the high diffusivities of alkalis in melt, reduced their initial spread in Al/Na (Fig. 15). Low diffusivities of Si and Al, however, are responsible for the spread in modal Qtz/feldspars, particularly of MI in Grt (Fig. 14), with higher Si in melts next to Qtz, and higher Al in those next to feldspars or peraluminous minerals.

Regarding trace elements, MI in both Pl and Grt show similar ranges and mean concentrations for those elements incompatible with their respective hosts. This suggests that, for the incompatible elements, MI (i) represent the compositions of the bulk matrix melt in the system at the time they were trapped, and (ii) matrix melt at this time had already a well-defined geochemical signature, with high concentrations of incompatible elements (highest Li, Cs, B, U/Th; lowest V, Zr, Th,

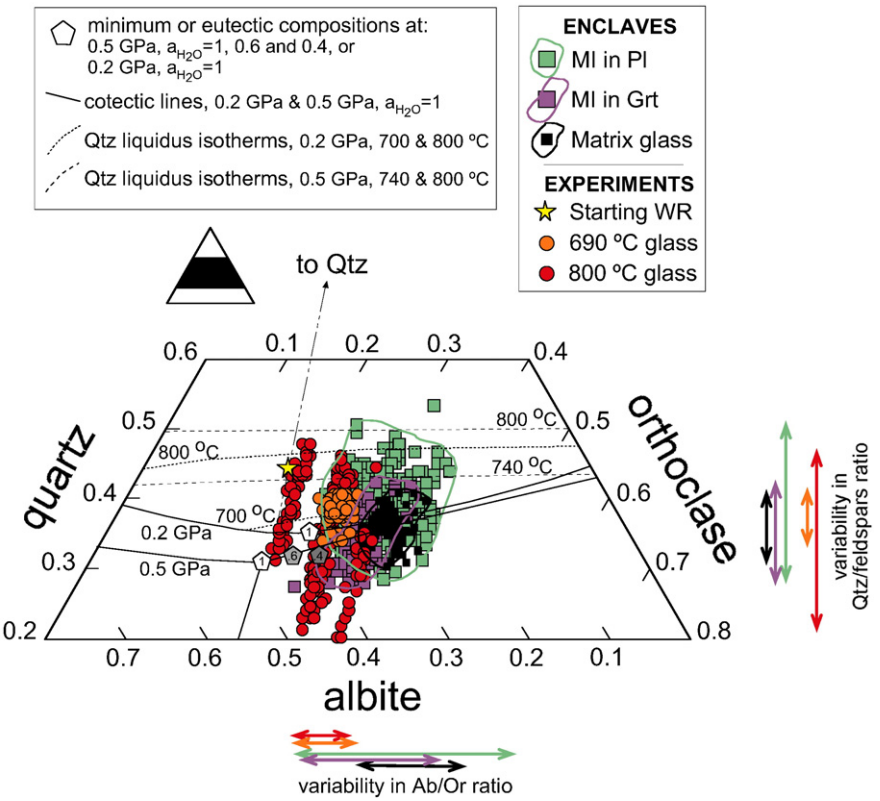

Fig. 14. Comparison between the wt% CIPW normative Qtz–Or–Ab compositions of glasses in El Hoyazo enclaves (separated as a function of microstructural location) and kinetics melting experiments (separated as a function of melting *T*). The experiments correspond to H_2O-saturated aplite core melting experiments at low (690 °C) and high (800 °C) degrees of T overstepping and 0.2 GPa. Haplogranitic minimum or eutectic points, cotectic lines and Qtz liquidus isotherms are from Tuttle and Bowen (1958) and Becker et al. (1998). Yellow start shows the whole rock composition of the starting aplite used in the kinetics melting experiments. Green, purple and black lines enclose the majority of analyses of MI in Pl, MI in Grt and matrix glass, respectively. Vertical and horizontal colored lines show the ranges in Qtz/feldspars and Ab/Or normative ratios, respectively, of glasses in each microstructural location or experimental *T*. See text for explanation.

REE) and, in general, more heterogeneous compositions than the current matrix glass (Acosta-Vigil et al., 2010). Based on Zr and LREE concentrations in glasses and Zrn and Mnz saturation thermometry, Acosta-Vigil et al. (2010) obtained an increase in T from ≈670–700 °C for MI in Pl, to 700–750 °C for MI in Grt, and up to 810 °C (though variable, ≈710–810 °C) for matrix glass. They also found that MI in Pl and MI in Grt are rich in trace elements strongly compatible in Ms, whereas matrix glass is enriched in minor and trace elements that are abundant in Bt. Hence, combining geochemistry and Zrn/Mnz saturation thermometry, and in accordance with estimations of H_2O in glass (H_2O by difference), they interpreted the MI in Pl and Grt to represent melts formed by the H_2O-present to H_2O-absent Ms-breakdown melting, whereas matrix glass constitutes melt formed at the beginning of the H_2O-absent Bt-breakdown melting.

Based on the trace element concentrations of MI, matrix glass and coexisting minerals, Acosta-Vigil et al. (2012b) obtained the following major conclusions on mineral–melt equilibration. (i) Using the concept of cross-partitioning concentration ratios introduced by these authors, they concluded that at the time of MI entrapment the matrix melt was likely interconnected and at, or close to equilibrium with most coexisting minerals, including Pl, Bt, Kfs. It was not, however, at equilibrium with Grt. And although already loaded with considerable quantities of Zr, Th and LREE, matrix melt was undersaturated to some extent in Zrn and Mnz. (ii) Right before extrusion and quenching, matrix melt and rims of most coexisting minerals were at equilibrium, but the extent of equilibrium between melt and bulk residue was likely being controlled by diffusion in melt. Melt and the mostly homogeneous (hence likely re-crystallized) Pl, Bt, Kfs and Crd were at equilibrium regarding fast diffusing Large Ion Lithophile Elements, whereas melt and Grt, Bt, Zrn and Mnz were at disequilibrium with respect to the slower diffusing First Row Transition Elements and High Field Strength Elements. Also, melt was to some extent undersaturated in Zrn, Mnz and hence the slow diffusing Rare Earth Elements. (iii) The process of bulk residue–melt equilibration is complex and its evolution may vary depending on minerals (variable capacity of recrystallization) and elements (variable diffusivities in minerals and melt). Overall, however, effective mineral–melt partition coefficients (K_{eff}) deviated from equilibrium ones (K_{eq}) in a different manner relative to that predicted by the model of Bea (1996), where $K_{eff} = 1$; this was likely due to extensive mineral re-crystallization contemporaneous with anatexis. (iv) Plagioclase, Bt, Kfs and Crd were in general at, or close to equilibrium with coexisting melt, whereas melt and Grt were not at equilibrium. This is likely due to re-crystallization of the former minerals — supported by their mostly homogeneous compositions in major and trace elements —, and lack of recrystallization of Grt — supported by heterogeneous composition along electron microprobe traverses, see Fig. 5 of Acosta-Vigil et al. (2010). (v) The observations that melt was at equilibrium either with most of the bulk residue (MI) or at least rims of minerals (matrix melt), that most minerals are homogeneous, and that bulk residue–matrix melt equilibrium seems controlled by diffusion in the melt, all support the conclusions based on major element chemistry (Fig. 14) that melting was diffusion-in-melt-controlled, and associated with a large *T* overstep of the reaction.

We notice that the anatectic scenario for the enclaves presented above, and obtained from the analysis of major and trace element concentrations of MI, matrix glass and coexiting minerals, is in accordance

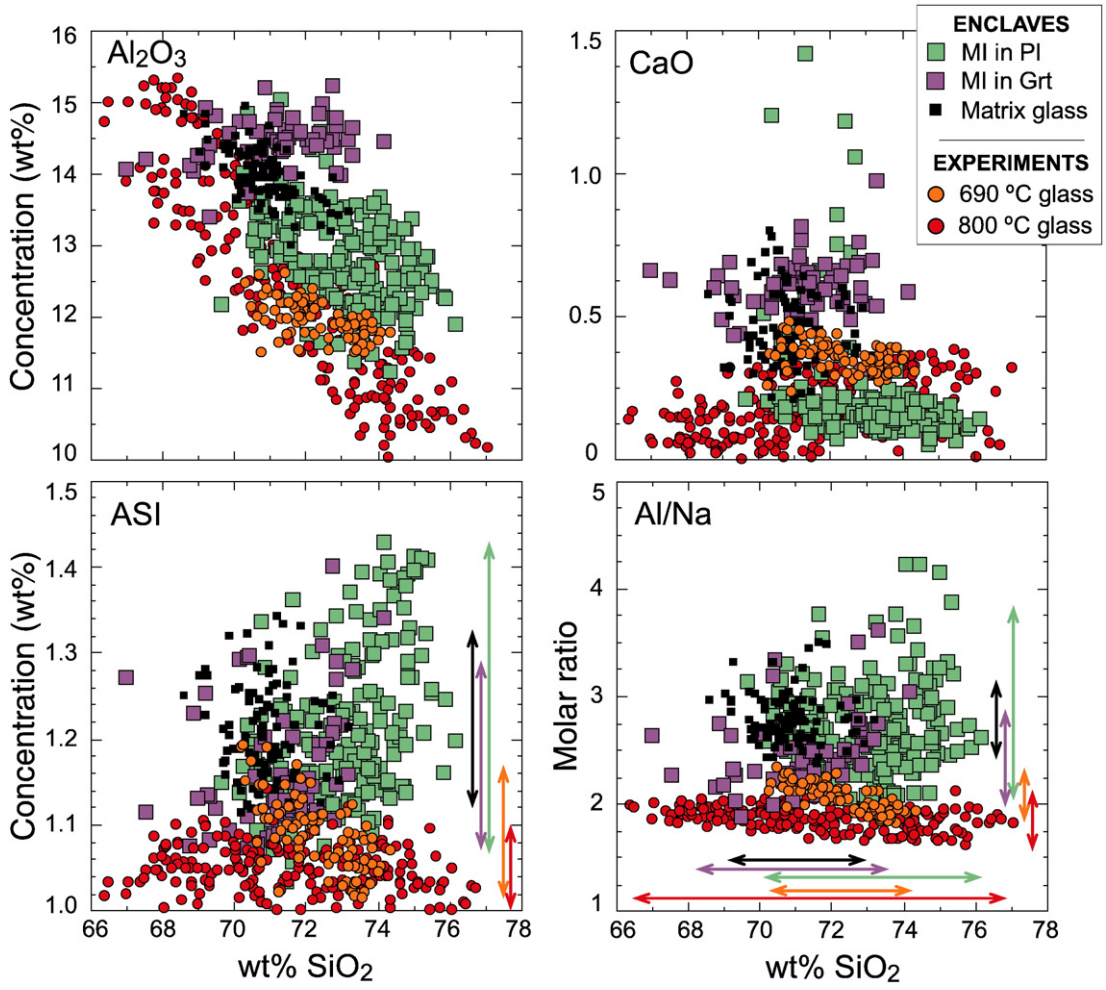

Fig. 15. Harker diagrams of glasses in El Hoyazo enclaves (as a function of microstructural location) and kinetics melting experiments (as a function of melting *T*). Vertical and horizontal colored lines show the ranges in Al/Na and ASI molar ratios, and SiO_2 concentrations, respectively, of glasses in each microstructural location or experimental *T*.

with the model proposed by Cesare and Maineri (1999) based on petrological (i.e. not geochemical) grounds: rapid *T* overstep melting and (re-)crystallization of a lower grade metamorphic rock. This shows the potential of this new approach.

5.4. Information from analyzed nanogranitoids (i.e. crystallized MI) in regional migmatites and granulites

Fig. 16 shows the Qtz–Or–Ab normative composition of all presently rehomogenized and analyzed nanogranitoids in migmatites and granulites, together with the experimental glasses produced during the granite core melting experiments and the glassy MI from El Hoyazo, for comparison. All nanogranitoids (≈420) are included in Grt and come from eight different rocks (protoliths are peraluminous metapelites and metagreywackes, and metaluminous orthogneisses and tonalites) collected in seven distinct anatectic terranes, that cover a variety of geologic/tectonic environments and *P*–*T*–a_{H2O} conditions: ≈660–700 to >900 °C, 0.45 to 2.7 GPa, and H_2O-rich fluid present to H_2O-poor fluid-present or fluid-absent scenarios (Table 2; see for details Acosta-Vigil et al., 2016; Bartoli et al., 2016a; Cesare et al., 2015; Ferrero et al., 2015).

In the Qtz–Or–Ab diagram, nanogranitoids plot mostly far from the haplogranite eutectics. They either tend to approach the degree of homogeneity shown by the experimental glasses produced at small degrees of overstepping (e.g. Ojén metatexites, La Galite), or show relatively heterogeneous compositions (e.g. OSBM, KGD, Jubrique granulites) (see also the discussion about MI homogeneity in Cesare et al., 2015). These more heterogeneous MI show, in addition, conspicuous trends with small variations in Ab/Or and large variations in Qtz/feldspar ratios, parallel to trends of experimental glasses produced at high degrees of overstepping.

Based on the comparison with experimental results on the kinetics of melting (Section 3), and assuming that pre- and post-entrapment processes have not affected the major element composition of analyzed MI, nanogranitoids in the Ojén metatexites and La Galite may approach cases (i.a) or (i.b) of Section 5.2. The trends shown by nanogranites from OSBM and, particularly KGD and the Jubrique diatexites, most likely reflect the control of diffusion in melt on the composition of interconnected melts (i.e. slow diffusion of Si and Al, extremely rapid diffusion of alkalis) [case (ii.c) of Section 5.2] and, hence, may suggest anatexis associated with high degrees of overstepping of the melt-producing reaction (Section 3.1.2). Further investigation on the nature of melting requires consideration of trace element data from MI and the coexisting minerals, and the compositional homogeneity of minerals (see case of El Hoyazo). In addition to the composition of the primary melts, other characteristics that might suggest overstepping of melting reactions in Nature are the frequently reported cases of rapid melt segregation in migmatites, necessarily implying rapid melting, and also the lack of textural equilibration; these observations seem at odds with a scenario of

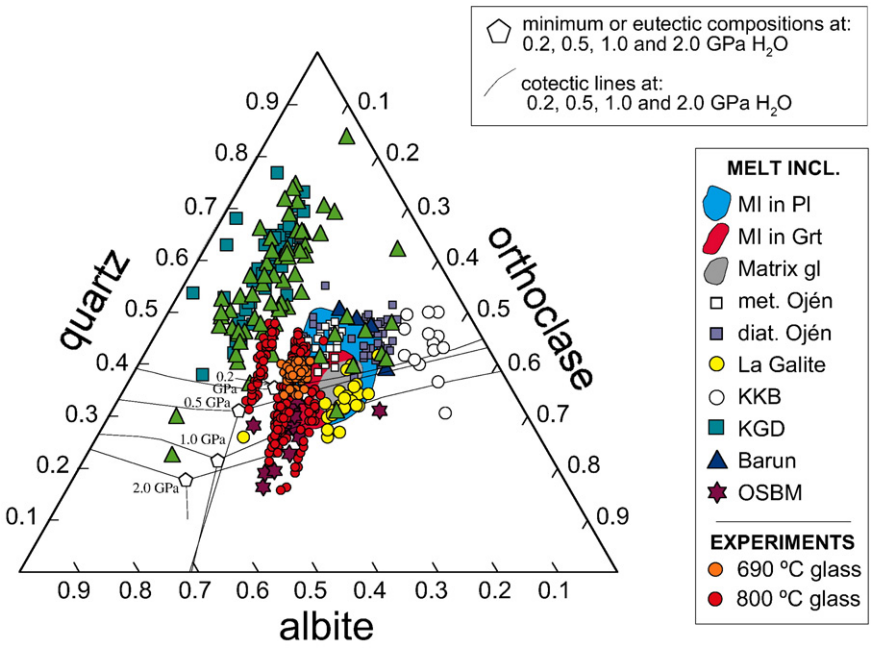

Fig. 16. Weight % CIPW normative Qtz–Or–Ab compositions of up-to-date rehomogenized and analyzed nanogranitoids in migmatites and granulites, together with granite core melting experimental glasses and analyzed glassy melt inclusions in Pl, melt inclusions in Grt and matrix glass from El Hoyazo anatectic enclaves. "met." refers to metatexites, and "diat." to diatexites. See text for explanation, and Table 2 for more information on the several case studies of nanogranitoids.
Modified from Fig. 13 of Cesare et al. (2015).

exceedingly slow melting during entirely rate of heating-controlled anatexis (see above).

A final but quite important observation is that, despite being in some cases relatively heterogeneous, nanogranitoids from each investigated scenario have a distinct composition that reflects the particular P–T–X–a_{H2O} conditions of the anatectic terrane, in other words the compositions recorded by nanogranitoids "capture" the environment of melting. For instance, nanogranitoids from ultra-high T rocks (KKB) approach the composition of the bulk rock (e.g. in Qtz–Or–Ab normative diagrams); nanogranites produced at H_2O-present conditions (KGD, Jubrique diatexites) are peraluminous granitoids displaced towards the Qtz–Ab sideline (compare with Conrad et al., 1988); nanogranitoids produced at lower T and H_2O-absent conditions plot towards the middle of the Qtz–Ab–Or diagram and closer to the haplogranitic eutectics, though melt composition is distinct for each specific case (see Cesare et al., 2015).

6. Concluding remarks

1. Together with Acosta-Vigil et al. (2010, 2012b), **this article establishes the basis for a new approach to investigate the nature, mechanisms and timing of crustal anatexis**, as well as controls on the composition of primary melts before segregation from the solid fraction, during particular case studies of migmatites. This is accomplished by combining data on equilibrium melting, the kinetics of melting, and melt inclusions in anatectic rocks. First, we use available experimental data on the kinetics of melting of crustal protoliths to provide a reference frame describing the processes acting during anatexis and their controls and inprint on melt compositions. Then, and after discussing the limitations of experiments to describe crustal anatexis in Nature, we test this experimental reference frame by using currently available analyses of primary melt inclusions in migmatites.

Table 2
Main characteristics of crustal anatexis in the reported cases of migmatites and granulites where nanogranitoids have been rehomogenized and analyzed.

Locality	Rock type	Assemblage	T, P conditions	Melting reaction	Reference
Kerala Khondalite Belt (India; KKB)	Felsic granulite	Qtz − Kfs − Grt − Crd − Sil − Bt − Spl	>900 °C, 0.6–0.8 GPa	H_2O-absent Bt-breakdown	Cesare et al. (2009)
Barun (Nepal)	Metasedimentary migmatite	Bt + Sil + Pl + Qtz + Grt	800–860 °C, 0.8 GPa	?	Ferrero et al. (2012)
Ojén, Ronda (Spain; met. Ojén)	Quartzo-feldspathic metatexite	Qtz − Pl − Kfs − Bt − Sil − Grt − Mus − Gr	660–700 °C, 0.45–0.5 GPa	H_2O-absent Ms- & Bt-breakdown	Bartoli et al. (2013a)
La Galite (Tunisia)	Tonalitic & garnetitic enclaves	Pl + Qtz + Grt + Bt + Kfs + Ilm; Grt + Qtz ± Kfs	770–820 °C, 0.5 GPa	H_2O-present Bt-breakdown	Ferrero et al. (2014)
Kali Gandaki (Nepal; KGD)	Metasedimentary granulites & migmatites	Qtz + P + Bt + Grt + Ky ± Sil	?	?	Carosi et al. (2015)
OS Dome, Bohemian Massif (OSBM)	Felsic granulite	Grt + Ky + Qtz + Msp + Pl + Rt	≥875 °C, 2.7 GPa	H_2O-absent hydrate-breakdown?	Ferrero et al. (2015)
Jubrique, Ronda (Spain)	Metapelitic granulite	Grt + Qtz + Pl + Kfs + Sil + Crd + Bt + Spl + Ilm	800 °C, ≤1.5 GPa	H_2O-present Bt-breakdown	Acosta-Vigil et al. (2016)
Ojén, Ronda (Spain; diat. Ojén)	Quartzo-feldspathic diatexite	Qtz − Pl − Kfs − Sil − Grt − Ilm − Bt − Gr	820 °C, 0.6 GPa	H_2O-absent Bt-breakdown	Bartoli et al. (2016b)

2. We emphasize that, even if the composition of melt inclusions trapped at a particular time is not entirely homogeneous and/or at equilibrium with the residue, **this does not mean either that melt inclusions are not recording primary melt compositions, or that they are not representative of the melt present in the migmatite during entrapment and useful to investigate anatexis in the rock** — provided that they have not been affected by processes operating at the interface (e.g. boundary layer phenomena) or post-entrapment modifications. This means that melt inclusions are able to "capture" (i) the anatectic environment where they form, and (ii) processes occurring in that particular migmatite during partial melting. This is the basis for using melt inclusion compositions to study the nature, mechanisms and timing of melting in migmatites.
3. Several processes may occur concomitantly during anatexis, including diffusion of heat through the protolith, reactions at mineral–melt interfaces, diffusion in melt and in minerals and recrystallization of minerals. Solid granite rock core melting experiments show that, during **anatexis at relatively low degrees of *T* overstepping** (≤10–60 °C), initial melts are quite homogeneous, close to the haplogranite minimum/eutectics, but at disequilibrium with the residue, which does not recrystallize. Though melting is fast and controlled by the rates of reactions at interfaces, melt–residue equilibration may take an extremely long time as it is controlled by diffusion in minerals, e.g. tens to hundreds of millions of years for Ca–Na in Pl, depending on the grain size. This scenario may apply to contact anatectic settings associated with relatively small overstepping of the melting reaction. Current microstructural and trace element geochemical studies on regional migmatites, documenting frequent disequilibrium features, suggest that this scenario might also apply to regional anatexis in collisional settings.
4. During **melting at high degrees of *T* overstepping** (≥100 °C), initial melts are heterogeneous and at equilibrium with the residue only at the mineral–melt interfaces. Minerals, however, quickly recrystallize. Hence melting, melt homogenization and mineral–residue equilibration time frames are much shorter as their rates are controlled by diffusion in the melt, e.g. tens of years for length scales of diffusion of ≈2 mm (associated with a minimum volume for equilibrium of 1 mm^3, Fig. 1b) for the case of H_2O-saturated anatexis. This scenario applies to contact anatectic settings, which can be present in important tectonic scenarios for the generation and differentiation of continental crust, such as the middle-to-lower crust above subduction zones and in continental rifts. It also applies during the rapid influx of H_2O-rich fluids in rocks that are already well above their wet solidus, and might apply during the first stages of regional anatexis in collisional orogens.
5. Comparison between the experimental reference frame and currently available melt inclusion data sets indicates that, in several cases were melt inclusion compositions are relatively homogeneous suggests that melting occurred either as (i) disequilibrium melting during contact anatexis at small degrees of temperature overstepping or during rate of heating-controlled regional anatexis; or (ii) equilibrium melting during contact anatexis at large degrees of temperature overstepping or during H_2O-fluxed melting of rocks well above their solidus, with enough time for melt–residue equilibration to occur between melt generation and entrapment as MI. Trace element studies on minerals are necessary to further confirm/investigate the nature of melting. In several cases melt inclusions are more heterogeneous and their compositions were likely controlled by diffusion in the melt, suggesting that melting occurred associated with a large temperature overstepping of the reaction.

Acknowledgements

This work was supported by the National Science Foundation [grants EAR-9603199, EAR-9618867, EAR-9625517 and EAR-9404658], the Italian Consiglio Nazionale delle Ricerche, the European Commission (grant 01-LECEMA22F through contract No. ERAS-CT-2003-980409; and a H2020 Marie Skłodowska-Curie Actions under grant agreement No. 654606), the Italian Ministry of Education, University and Research (grants PRIN 2007278A22, 2010TT22SC and SIR RBSI14Y7PF), the Università degli Studi di Padova [Progetto di Ateneo CPDA107188/10 and a Piscopia—Marie Curie Fellowship under grant agreement No. 600376], the Australian Research Council (Australian Professorial Fellowship and Discovery Grants Nos. DP0342473 and DP0556700), and the National Research Foundation (South Africa; Incentives For Rated Researchers Program). The research leading to these results has received funding from the European Commission, Seventh Framework Programme, under Grant Agreement No. 600376. This project has received funding from the European Union's Horizon 2020 research and innovation programme under the Marie Sklodowska-Curie grant agreement No. 654606. We are grateful to Edward Sawyer for his editorial work, and to Bruce Watson, Cliff Shaw and an anonymous reviewer for their thorough and thoughtful reviews that greatly improved the clarity and consistency of the manuscript.

References

Acosta-Vigil, A., London, D., Dewers, T.A., Morgan VI, G.B., 2002. Dissolution of corundum and andalusite in H_2O-saturated haplogranitic melts at 800 °C and 200 MPa: constraints on diffusivities and the generation of peraluminous melts. Journal of Petrology 43, 1885–1908.

Acosta-Vigil, A., London, D., Morgan VI, G.B., Dewers, T.A., 2003. Solubility of excess alumina in hydrous granitic melts in equilibrium with peraluminous minerals at 700–800 °C and 200 MPa, and applications of the aluminum saturation index. Contributions to Mineralogy and Petrology 146, 100–119.

Acosta-Vigil, A., London, D., Morgan VI, G.B., 2005. Contrasting interactions of sodium and potassium with H_2O in haplogranitic liquids and glasses at 200 MPa from hydration-diffusion experiments. Contributions to Mineralogy and Petrology 149, 276–287.

Acosta-Vigil, A., London, D., Morgan VI, G.B., 2006a. Experiments on the kinetics of partial melting of a leucogranite at 200 MPa H_2O and 690–800 °C: compositional variability of melts during the onset of H_2O-saturated crustal anatexis. Contributions to Mineralogy and Petrology 151, 539–557.

Acosta-Vigil, A., London, D., Morgan VI, G.B., Dewers, T.A., 2006b. Dissolution of quartz, albite, and orthoclase in H_2O-saturated haplogranitic melts at 800 °C and 200 MPa: diffusive transport properties of granitic melts at crustal anatectic conditions. Journal of Petrology 47, 231–254.

Acosta-Vigil, A., Cesare, B., London, D., Morgan VI, G.B., 2007. Microstructures and composition of melt inclusions in a crustal anatectic environment, represented by metapelitic enclaves within El Hoyazo dacites, SE Spain. Chemical Geology 235, 450–465.

Acosta-Vigil, A., Buick, I., Hermann, J., Cesare, B., Rubatto, D., London, D., Morgan VI, G.B., 2010. Mechanisms of crustal anatexis: a geochemical study of partially melted metapelitic enclaves and host dacite, SE Spain. Journal of Petrology 51, 785–821.

Acosta-Vigil, A., London, D., Morgan VI, G.B., 2012a. Chemical diffusion of major components in granitic liquids: implications for the rates of homogenization of crustal melts. Lithos 153, 308–323.

Acosta-Vigil, A., Buick, I., Cesare, B., London, D., Morgan VI, G.B., 2012b. The extent of equilibration between melt and residuum during regional anatexis and its implications for differentiation of the continental crust: a study of partially melted metapelitic enclaves. Journal of Petrology 53, 1319–1356.

Acosta-Vigil, A., Barich, A., Bartoli, O., Garrido, C., Cesare, B., Remusat, L., Poli, S., Raepsaet, C., 2016. The composition of nanogranitoids in migmatites overlying the Ronda peridotites (Betic Cordillera, S Spain): the anatectic history of a polymetamorphic basement. Contributions to Mineralogy and Petrology http://dx.doi.org/10.1007/s00410-016-1230-3.

Albarede, F., Bottinga, Y., 1972. Kinetic disequilibrium in trace element partitioning between phenocrysts and host lava. Geochimica et Cosmochimica Acta 36, 141–156.

Anczkiewicz, R., Chakraborty, S., Dasgupta, S., Mukhopadhyay, D., Koltonik, K., 2014. Timing, duration and inversion of prograde Barrovian metamorphism constrained by high resolution Lu-Hf garnet dating: a case study from the Sikkim Himalaya, NE India. Earth and Planetary Science Letters 407, 70–81.

Annen, C., Sparks, R.S.J., 2002. Effects of repetitive emplacement of basaltic intrusions on thermal evolution and melt generation in the crust. Earth and Planetary Science Letters 203, 937–955.

Annen, C., Blundy, J.D., Sparks, R.S.J., 2006. The genesis of intermediate and silicic magmas in deep crustal hot zones. Journal of Petrology 47, 505–539.

Arzi, A.A., 1978. Fusion kinetics, water pressure, water diffusion and electrical conductivity in melting rock, interrelated. Journal of Petrology 19, 153–169.

Audetat, A., Lowenstern, J.B., 2013. Melt inclusions. In: Holland, H.D., Turekian, K.K. (Eds.), Treatise on Geochemistry, 2nd edn. Elsevier, Oxford, pp. 143–173.

Baker, D.R., 1990. Chemical interdiffusion of dacite and rhyolite: anhydrous measurements at 1 atm and 10 kbar, application of transition state theory, and diffusion in zoned magma chambers. Contributions to Mineralogy and Petrology 104, 407–423.

Baker, D.R., 1991. Interdiffusion of hydrous dacitic and rhyolitic melts and the efficacy of rhyolite contamination of dacitic enclaves. Contributions to Mineralogy and Petrology 106, 462–473.

Baker, D.R., 2008. The fidelity of melt inclusions as records or melt composition. Contributions to Mineralogy and Petrology 156, 377–395.

Barbero, L., Villaseca, C., Rogers, G., Brown, P.E., 1995. Geochemical and isotopic disequilibrium in crustal melting: an insight from the anatectic granitoids from Toledo, Spain. Journal of Geophysical Research 100, 15745–15765.

Barbey, P., Bertrand, J.-M., Angoua, S., Dautel, D., 1989. Petrology and U/Pb geochronology of the Telohat migmatites, Aleksod, Central Hoggar, Algeria. Contributions to Mineralogy and Petrology 101, 207–219.

Barich, A., Acosta-Vigil, A., Garrido, J.C., Cesare, B., Tajčmanová, L., Bartoli, O., 2014. Microstructures and petrology of melt inclusions in the anatectic sequence of Jubrique (Betic Cordillera, S Spain): implications for crustal anatexis. Lithos 206–207, 303–320.

Barr, D., 1985. Migmatites in the Moines. In: Ashworth, J.R. (Ed.), Migmatites. Blackie, Glasgow, pp. 225–264.

Bartoli, O., Tajčmanová, L., Cesare, B., Acosta-Vigil, A., 2013a. Phase equilibria constraints on melting of stromatic migmatites from Ronda (S. Spain): insights on the formation of peritectic garnet. Journal of Metamorphic Geology 31, 775–789.

Bartoli, O., Cesare, B., Poli, S., Acosta-Vigil, A., Esposito, R., Turina, A., Bodnar, R.J., Angel, R.J., Hunter, J., 2013b. Nanogranite inclusions in migmatitic garnet: behavior during piston cylinder re-melting experiments. Geofluids 13, 405–420.

Bartoli, O., Cesare, B., Poli, S., Bodnar, R.J., Acosta-Vigil, A., Frezzotti, M.L., Meli, S., 2013c. Recovering the composition of melt and the fluid regime at the onset of crustal anatexis and S-type granite formation. Geology 41, 115–118.

Bartoli, O., Cesare, B., Remusat, L., Acosta-Vigil, A., Poli, S., 2014. The H_2O content of granite embryos. Earth and Planetary Science Letters 395, 281–290.

Bartoli, O., Acosta-Vigil, A., Cesare, B., 2015. High temperature metamorphism and crustal melting: working with melt inclusions. Periodico di Mineralogia 84. http://dx.doi.org/10.2451/2015PM00xx.

Bartoli, O., Acosta-Vigil, A., Ferrero, S., Cesare, B., 2016a. Granitoid magmas preserved as melt inclusions in high-grade metamorphic rocks. American Mineralogist 101, 1543–1559.

Bartoli, O., Acosta-Vigil, A., Tajčmanová, L., Cesare, B., Bodnar, R.J., 2016b. Using nanogranitoids and phase equilibria modeling to unravel anatexis in the crustal footwall of the Ronda peridotites (Betic Cordillera, S Spain). Lithos 256–257, 282–299.

Baschek, G., Johannes, W., 1995. The estimation of NaSi-CaAl interdiffusion rates in peristerite by homogenization experiments. European Journal of Mineralogy 7, 295–307.

Bea, F., 1991. Geochemical modeling of low melt-fraction anatexis in a peraluminous system: the Peña Negra Complex (central Spain). Geochimica et Cosmochimica Acta 55, 1859–1874.

Bea, F., 1996. Controls on the trace element composition of crustal melts. Transactions of the Royal Society of Edinburgh: Earth Sciences 87, 33–41.

Becker, A., Holtz, F., Johannes, W., 1998. Liquidus temperatures and phase compositions in the system Qz-Ab-Or at 5 kbar and very low water activities. Contributions to Mineralogy and Petrology 130, 213–224.

Brady, J.B., Cherniak, D.J., 2010. Diffusion in minerals: an overview of published experimental diffusion data. In: Zhang, Y., Cherniak, D.J. (Eds.), Diffusion in Minerals and Melts. Reviews in Mineralogy and Geochemistry vol. 72, pp. 899–920.

Brearley, A.J., Rubie, D.C., 1990. Effects of H_2O on the disequilibrium breakdown of muscovite + quartz. Journal of Petrology 31, 925–956.

Brown, M., 2002. Retrograde processes in migmatites and granulites revisited. Journal of Metamorphic Geology 20, 25–40.

Brown, M., 2010. The spatial and temporal patterning of the deep crust and implications for the process of melt extraction. Philosophical Transactions of the Royal Society 368, 11–51.

Brown, M., 2013. Granite: from genesis to emplacement. Geological Society of America Bulletin 125, 1079–1113.

Brown, C.R., Yakymchuk, C., Brown, M., Fanning, C.M., Korhonen, F.J., Piccoli, P.M., Siddoway, C.S., 2016. From source to sink: petrogenesis of Cretaceous anatectic granites from the Fosdick migmatite-granite complex, West Antarctica. Journal of Petrology 57, 1241–1278.

Buick, I.S., Stevens, G., Gibson, R.L., 2004. The role of water retention in the anatexis of metapelites in the Bushveld Complex Aureole, South Africa: an experimental study. Journal of Petrology 45, 1777–1797.

Carosi, R., Montomoli, C., Langone, A., Turina, A., Cesare, B., Iaccarino, S., Fascioli, L., Visonà, D., Ronchi, A., Santa Man, R., 2015. Eocene partial melting recorded in peritectic garnets from kyanite-gneiss, Greater Himalayan Sequence, central Nepal. In: Mukherjee, S., Carosi, R., van der Beek, P.A., Mukherjee, B.K., Robinson, D.M. (Eds.), Tectonics of the Himalaya. Geological Society, London, Special Publications 412, pp. 111–129.

Carvalho, B.B., Sawyer, E.W., Janasi, V.A., 2016. Crustal reworking in a shear zone: transformation of metagranite to migmatite. Journal of Metamophic Geology http://dx.doi.org/10.1111/jmg.12180.

Cesare, B., 2008. Crustal melting: working with enclaves. In: Sawyer, E.W., Brown, M. (Eds.), Working With Migmatites. Mineralogical Association of Canada, Montreal, Short Course vol. 38, pp. 37–55.

Cesare, B., Acosta-Vigil, A., 2011. Using Melt Inclusions for Understanding Crustal Melting Processes. McGraw-Hill Yearbook of Science & Technology, pp. 355–359.

Cesare, B., Gómez-Pugnaire, M.T., 2001. Crustal melting in the Alborán domain: constraints from enclaves of the Neogene Volcanic Province. Physics and Chemistry of the Earth 26, 255–260.

Cesare, B., Maineri, C., 1999. Fluid-present anatexis of metapelites at El Joyazo (SE Spain): constraints from Raman spectroscopy of graphite. Contributions to Mineralogy and Petrology 135, 41–52.

Cesare, B., Salvioli-Mariani, E., Venturelli, G., 1997. Crustal anatexis and melt extraction during deformation in the restitic xenoliths at El Joyazo (SE Spain). Mineralogical Magazine 61, 15–27.

Cesare, B., Ferrero, S., Salvioli-Mariani, E., Pedron, D., Cavallo, A., 2009. Nanogranite and glassy inclusions: the anatectic melt in migmatites and granulites. Geology 37, 627–630.

Cesare, B., Acosta-Vigil, A., Ferrero, S., Bartoli, O., 2011. Melt inclusions in migmatites and granulites. In: Forster, M.A., Fitz Gerald, J.D. (Eds.), The Science of Microstructure – Part II. Journal of the Virtual Explorer Electronic Edition (ISSN 1441-8142, 38, paper 2).

Cesare, B., Acosta-Vigil, A., Bartoli, O., Ferrero, S., 2015. What can we learn from melt inclusions in migmatites and granulites? Lithos 239, 186–216.

Chakraborty, S., 1995. Diffusion in silicate melts. In: Stebbins, J.F., McMillan, P.F., Dingwell, D.B. (Eds.), Structure, Dynamics, and Properties of Silicate Melts. Reviews in Mineralogy and Geochemistry vol. 32, pp. 409–503.

Chakraborty, S., Ganguly, J., 1992. Cation diffusion in aluminosilicate garnets: experimental determination in spessartine-almandine diffusion couples, evaluation of effective binary diffusion coefficients, and applications. Contributions to Mineralogy and Petrology 111, 74–86.

Chakraborty, S., Rubie, D.C., 1996. Mg tracer diffusion in aluminosilicate garnets at 750–850 °C, 1 atm and 1300 °C, 8.5 GPa. Contributions to Mineralogy and Petrology 122, 406–414.

Chakraborty, S., Dingwell, D.B., Rubie, D.C., 1995. Multicomponent diffusion in ternary silicate melts in the system K_2O-Al_2O_3-SiO_2: I. Experimental measurements. Geochimica et Cosmochimica Acta 59, 225–264.

Chappell, B.W., 1996. Magma mixing and the production of compositional variation within granite suites: evidence from the granites of southeastern Australia. Journal of Petrology 37, 449–470.

Chappell, B.W., White, A.J.R., 1992. I- and S-type granites in the Lachlan Fold Belt. Transactions of the Royal Society of Edinburgh: Earth Sciences 83, 1–26.

Chappell, B.W., White, A.J.R., Wyborn, D., 1987. The importance of residual source material (restite) in granite petrogenesis. Journal of Petrology 28, 1111–1138.

Cherniak, D.J., 1996. Strontium diffusion in sanidine and albite, and general comments on Sr diffusion in alkali feldspars. Geochimica et Cosmochimica Acta 60, 5037–5043.

Cherniak, D.J., 2002. Ba diffusion in feldspar. Geochimica et Cosmochimica Acta 66, 1641–1650.

Cherniak, D.J., 2005. Yb and Y diffusion in grossular garnet. Geochimica et Cosmochimica Acta 69, 405.

Cherniak, D.J., Watson, E.B., 1992. A study of strontium diffusion in K-feldspar, NaK feldspar and anorthite using Rutherford Backscattering Spectroscopy. Earth and Planetary Science Letters 113, 411–425.

Cherniak, D.J., Watson, E.B., 1994. A study of strontium diffusion in plagioclase using Rutherford backscattering spectroscopy. Geochimica et Cosmochimica Acta 58, 5179–5190.

Clemens, J.D., 2006. Melting of the continental crust: fluid regimes, melting reactions, and source-rock fertility. In: Brown, M., Rushmer, T. (Eds.), Evolution and Differentiation of the Continental Crust. Cambridge University Press, pp. 296–331.

Clemens, J.D., 2009. The message in the bottle: "Melt" inclusions in migmatitic garnets. Geology 37, 671–672.

Clemens, J.D., Benn, K., 2010. Anatomy, emplacement and evolution of a shallow-level, post-tectonic laccolith: the Mt Disappointment pluton, SE Australia. Journal of the Geological Society of London 167, 915–941.

Clemens, J.D., Vielzeuf, D., 1987. Constraints on melting and magma production in the crust. Earth and Planetary Science Letters 86, 287–306.

Clemens, J.D., Watkins, J.M., 2001. The fluid regime of high-temperature metamorphism during granitoid magma genesis. Contributions to Mineralogy and Petrology 140, 600–606.

Collins, W.J., 1996. Lachlan Fold Belt granitoids: products of three-component mixing. Transactions of the Royal Society of Edinburgh: Earth Sciences 87, 171–181.

Conrad, W.K., Nicholls, I.A., Wall, V.J., 1988. Water-saturated and -undersaturated melting of metaluminous and peraluminous crustal compositions at 10 kb: evidence for the origin of silicic magmas in the Taupo Volcanic Zone, New Zealand, and other occurrences. Journal of Petrology 29, 765–803.

Cooper, A.R., 1968. The use and limitations of the concept of an effective binary diffusion coefficient for multicomponent diffusion. In: Wachtman, J.B., Franklin, A.D. (Eds.), Mass Transport in Oxides. NBS Special Publications vol. 296, pp. 79–84.

Crank, J., 1975. The Mathematics of Diffusion. Oxford University Press, Oxford.

De Yoreo, J.J., Lux, D.R.T., Guidotti, C.V., Decker, E.R., Osberg, P.H., 1989. The Acadian thermal history of western Maine. Journal of Metamorphic Geology 7, 169–190.

Deniel, C., Vidal, P., Fernandez, A., LeFort, P., Pecaut, J.J., 1987. Isotopic study of the Manaslu granite (Himalaya, Nepal): inferences of the age and source of Himalayan leucogranites. Contributions to Mineralogy and Petrology 96, 78–92.

Dufek, J., Bergantz, G.W., 2005. Lower crustal magma genesis and preservation: a stochastic framework for the evaluation of basalt–crust interaction. Journal of Petrology 46, 2167–2195.

Ferrero, S., Bartoli, O., Cesare, B., Salvioli-Mariani, E., Acosta-Vigil, A., Cavallo, A., Groppo, C., Battiston, S., 2012. Microstructures of melt inclusions in anatectic metasedimentary rocks. Journal of Metamorphic Geology 30, 303–322.

Ferrero, S., Braga, R., Berkesi, M., Cesare, B., Laridhi Ouazaa, N., 2014. Production of metaluminous melt during fluid-present anatexis: an example from the Maghrebian basement, La Galite Archipelago, central Mediterranean. Journal of Metamorphic Geology 32, 209–225.

Ferrero, S., Wunder, B., Walczak, K., O'Brien, P.J., Ziemann, M.A., 2015. Preserved near ultrahigh-pressure melt from continental crust subducted to mantle depths. Geology 43, 447–450.

Foland, K.A., 1974. Alkali diffusion in orthoclase. In: Hofmann, A.W., Giletti, B.J., Yoder Jr., H.S., Yund, R.A. (Eds.), Geochemical Transport and Kinetics. Carnegie Institution of Washington, Washington, pp. 77–98.
Freer, R., Edwards, A., 1999. An experimental study of Ca-(Fe,Mg) interdiffusion in silicate garnets. Contributions to Mineralogy and Petrology 134, 370–379.
Frezzotti, M.L., Ferrando, S., 2015. The chemical behavior of fluids released during deep subduction based on fluid inclusions. American Mineralogist 100, 352–377.
García-Arias, M., Stevens, G., 2017. Phase equilibrium modelling of granite magma petrogenesis: A. An evaluation of the magma compositions produced by crystal entrainment in the source. Lithos 277, 131–153.
Giletti, B.J., Casserly, J.E.D., 1994. Strontium diffusion kinetics in plagioclase feldspars. Geochimica et Cosmochimica Acta 58, 3785–3793.
Glazner, A.F., Bartley, J.M., Coleman, D.S., Gray, W., Taylor, R.Z., 2004. Are plutons assembled over millions of years by amalgamation from small magma chambers? GSA Today 14, 4–11.
Grant, J.A., 2009. THERMOCALC and experimental modelling of pelite, Morton Pass, Wyoming. Journal of Metamorphic Geology 27, 571–578.
Gray, C.M., Kemp, A.I.S., 2009. The two-component model for the genesis of granitic rocks in southeastern Australia — nature of the metasedimentary-derived and basaltic end members. Lithos 111, 113–124.
Grove, T.L., Baker, M.B., Kinzler, R.J., 1984. Coupled CaAl-NaSi diffusion in plagioclase feldspar: experiments and applications to cooling rate speedometry. Geochimica et Cosmochimica Acta 48, 2113–2121.
Harris, N., Ayres, M., Massey, J., 1995. Geochemistry of granitic melts produced during the incongruent melting of muscovite: implications for the extraction of Himalayan leucogranite magmas. Journal of Geophysical Research 100, 15767–15777.
Harris, N., Vance, D., Ayres, M., 2000. From sediment to granite: timescales of anatexis in the upper crust. Chemical Geology 162, 155–167.
Hermann, J., Rubatto, D., 2003. Relating zircon and monazite domains to garnet growth zones: age and duration of granulite facies metamorphism in the Val Malenco lower crust. Journal of Metamorphic Geology 21, 833–852.
Hodges, K.V., LeFort, P., Pecher, A., 1988. Possible thermal buffering by crustal anatexis in collisional orogens: thermobarometric evidence from the Nepalese Himalaya. Geology 16, 707–710.
Hogan, J.P., Sinha, A.K., 1991. The effect of accessory minerals on the redistribution of lead isotopes during crustal anatexis: a model. Geochimica et Cosmochimica Acta 55, 335–348.
Holness, M.B., 2010. Decoding dihedral angles in melt-bearing and solidified rocks. In: Forster, M.A., Fitz Gerald, J.D. (Eds.), The Science of Microstructure — Part I. Journal of the Virtual Explorer Electronic Edition (ISSN 1441-8142, 35, paper 2).
Holness, M.B., Sawyer, E.W., 2008. On the pseudomorphing of melt-filled pores during the crystallization of migmatites. Journal of Petrology 49, 1343–1363.
Holness, M.B., Dane, K., Sides, R., Richardson, C., Caddick, M., 2005. Melting and melt segretation in the aureole of the Glenmore Plug, Ardnamurchan. Journal of Metamorphic Geology 23, 29–43.
Holtz, F., Johannes, W., Tamic, N., Behrens, H., 2001. Maximum and minimum water contents of granitic melts generated in the crust: a reevaluation and implications. Lithos 56, 1–14.
Holyoke III, C.W., Rushmer, T., 2002. An experimental study of grain scale melt segregation mechanisms in two common crustal rock types. Journal of Metamorphic Geology 20, 493–512.
Hwang, S.-L., Shen, P., Chu, H.-T., Yui, T.-F., Lin, C.-C., 2001. Genesis of microdiamonds from melt and associated multiphase inclusions in garnet of ultrahigh-pressure gneiss from Erzgebirge, Germany. Earth and Planetary Science Letters 188, 9–15.
Icenhower, J., London, D., 1995. An experimental study of element partitioning among biotite, muscovite, and coexisting peraluminous silicic melt at 200 MPa (H_2O). American Mineralogist 80, 1229–1251.
Jin, Z., Green, H.W., Zhou, Y., 1994. Melt topology in partially molten mantle peridotite during ductil deformation. Nature 372, 164–167.
Johannes, W., 1980. Metastable melting in the granite system Qz-Or-Ab-An-H_2O. Contributions to Mineralogy and Petrology 72, 73–80.
Johannes, W., 1989. Melting of plagioclase-quartz assemblages at 2 kbar water pressure. Contributions to Mineralogy and Petrology 103, 270–276.
Johannes, W., Holtz, F., 1992. Melting of plagioclase in granite and related systems: composition of coexisting phases and kinetic observations. Transactions of the Royal Society of Edinburgh: Earth Sciences 83, 417–422.
Johannes, W., Koepke, J., 2001. Incomplete reaction of plagioclase in experimental dehydration melting of amphibolite. Australian Journal of Earth Sciences 48, 581–590.
Kent, A.J.R., 2008. Melt inclusions in basaltic and related volcanic rocks. Reviews in Mineralogy and Geochemistry 69, 273–331.
Korsakov, A.V., Hermann, J., 2006. Silicate and carbonate melt inclusions associated with diamonds in deeply subducted carbonate rocks. Earth and Planetary Science Letters 241, 104–118.
Kretz, R., 1983. Symbols for rock-forming minerals. American Mineralogist 68, 277–279.
Liang, Y., 1999. Diffusive dissolution in ternary systems: analysis with applications to quartz and quartzite dissolution in molten silicates. Geochimica et Cosmochimica Acta 63, 3983–3995.
Liang, Y., 2000. Dissolution in molten silicates: effects of solid solution. Geochimica et Cosmochimica Acta 64, 1617–1627.
Liang, Y., 2003. Kinetics of crystal-melt reaction in partially molten silicates: 1. Grain scale processes. Geochemistry, Geophysics, Geosystems 4:1–27. http://dx.doi.org/10.1029/2002GC000375.
Liang, Y., 2010. Multicomponent diffusion in molten silicates: theory, experiments, and geological applications. In: Zhang, Y., Cherniak, D.J. (Eds.), Diffusion in Minerals and Melts. Reviews in Mineralogy and Geochemistry vol. 72, pp. 409–446.
Liu, M., Yund, R.A., 1992. NaSi-CaAl interdiffusion in plagioclase. American Mineralogist 77, 275–283.
London, D., 2008. Pegmatites. The Canadian Mineralogist Special Publication 10. NRC Research Press, Ottawa, Ontario, Canada.
London, D., 2009. The origin of primary textures in granitic pegmatites. Canadian Mineralogist 47, 697–724.
London, D., 2014. A petrological assessment of internal zonation in granitic pegmatites. Lithos 184–187, 74–104.
London, D., Morgan VI, G.B., Acosta-Vigil, A., 2012. An experimental simulation of assimilation of metapelite by granitic melt. Lithos 153, 292–307.
Loomis, T.P., Ganguly, J., Elphick, S.C., 1985. Experimental determination of cation diffusivities in aluminosilicate garnets; II, multicomponent simulation and tracer diffusion coefficients. Contributions to Mineralogy and Petrology 90, 45–51.
Mehnert, K.R., 1968. Migmatites and the Origin of Granitic Rocks. Elsevier, Amsterdam.
Mehnert, K.R., Büsch, W., Schneider, G., 1973. Initial melting at grain boundaries of quartz and feldspars in gneisses and granulites. Neues Jahrbuch für Mineralogie Monatshefte 4, 165–183.
Milord, I., Sawyer, E.W., Brown, M., 2001. Formation of diatexite migmatite and granite magma during anatexis of semi-pelitic metasedimentary rocks: an example from St. Malo, France. Journal of Petrology 42, 487–505.
Morfin, S., Sawyer, E.W., Bandyayera, D., 2014. The geochemical signature of a felsic injection complex in the continental crust: Opinaca Subprovince, Quebec. Lithos 196–197, 339–355.
Morgan VI, G.B., Acosta-Vigil, A., London, D., 2008. Diffusive equilibration between hydrous metaluminous–peraluminous haplogranitic liquid couples at 200 MPa (H_2O) and alkali transport in granitic liquids. Contributions to Mineralogy and Petrology 155, 257–269.
Mungall, J.E., Romano, C., Dingwell, D.B., 1998. Multicomponent diffusion in the molten system K_2O-Na_2O-Al_2O_3-SiO_2-H_2O. American Mineralogist 83, 685–699.
Nakamura, M., Shimakita, S., 1998. Dissolution origin and syn-entrapment compositional change of melt inclusion in plagioclase. Earth and Planetary Science Letters 161, 119–133.
Perchuk, A.L., Burchard, M., Schertl, H.-P., Maresch, W.V., Gerya, T.V., Bernhardt, H.-J., Vidal, O., 2009. Diffusion of divalent cations in garnet. Contributions to Mineralogy and Petrology 157, 573–592.
Powell, R., Downes, J., 1990. Garnet porphyroblast-bearing leucosomes in metapelites: mechanisms, phase diagrams, and an example from Broken Hill, Australia. In: Ashworth, J.R., Brown, M. (Eds.), High-Temperature Metamorphism and Crustal Anatexis. Unwin Hyman, London, pp. 105–123.
Pressley, R.A., Brown, M., 1999. The Phillips pluton, Maine, USA: evidence of heterogeneous crustal sources and implications for granite ascent and emplacement mechanisms in convergent orogens. Lithos 46, 335–366.
Roedder, E., 1984. Fluid inclusions. Reviews in Mineralogy 12, 1–644.
Rosenberg, C.L., Riller, U., 2000. Partial-melt topology in statically and dynamically recrystallized granite. Geology 28, 7–10.
Rubie, D.C., 1998. Disequilibrium during metamorphism: the role of nucleation kinetics. In: Treloar, P.J., O'Brien, P.J. (Eds.), What Drives Metamorphism and Metamorphic Reactions? Geological Society, London, Special Publications 138, pp. 199–214.
Rubie, D.C., Brearley, A.J., 1990. A model for rates of disequilibrium melting during metamorphism. In: Ashworth, J.R., Brown, M. (Eds.), High Temperature Metamorphism and Crustal Anatexis. Unwin Hyman, London, pp. 57–86.
Rudnick, R.L., Gao, S., 2003. The composition of the continental crust. In: Holland, H.D., Turekian, K.K. (Eds.), Treatise on Geochemistry. The Crust 3. Elsevier-Pergamon, Oxford, pp. 1–64.
Rushmer, T., 1995. An experimental deformation study of partially molten amphibolite: application to low-fraction melt segregation. Journal of Geophysical Research 100, 15681–15696.
Rushmer, T., 2001. Volume change during partial melting reactions: implications for melt extraction, melt geochemistry and crustal rheology. Tectonophysics 342, 389–405.
Rutter, E., Neumann, D., 1995. Experimental deformation of partially molten Westerly granite under fluid-absent conditions with implications for the extraction of granitic magmas. Journal of Geophysical Research 100, 15697–15715.
Sawyer, E.W., 1987. The role of partial melting and fractional crystallization in determining discordant migmatite leucosome compositions. Journal of Petrology 28, 445–473.
Sawyer, E.W., 1991. Disequilibrium melting and the rate of melt-residuum separation during migmatization of mafic rocks from the Grenville Front, Quebec. Journal of Petrology 32, 701–738.
Sawyer, E.W., 1998. Formation and evolution of granite magmas during crustal reworking: the significance of diatexites. Journal of Petrology 39, 1147–1167.
Sawyer, E.W., 1999. Criteria for the recognition of partial melting. Physics and Chemistry of the Earth 24, 269–279.
Sawyer, E.W., 2001. Melt segregation in the continental crust: distribution and movement of melt in anatectic rocks. Journal of Metamorphic Geology 19, 291–309.
Sawyer, E.W., 2008. Atlas of Migmatites. The Canadian Mineralogist Special Publication 9. NRC Research Press, Ottawa, Ontario, Canada.
Sawyer, E.W., 2010. Migmatites formed by water-fluxed partial melting of a leucogranodiorite protolith: microstructures in the residual rocks and source of the fluid. Lithos 116, 273–286.
Sawyer, E.W., 2014. The inception and growth of leucosomes: microstructure at the start of melt segregation in migmatites. Journal of Metamorphic Geology 32, 695–712.
Shaw, C.S.J., 2004. Mechanisms and rates of quartz dissolution in melts in the CMAS (CaO-MgO-Al_2O_3-SiO_2) system. Contributions to Mineralogy and Petrology 148, 180–200.
Solar, G.S., Brown, M., 2001. Petrogenesis of migmatites in Maine, USA: possible source of peraluminous leucogranite in plutons? Journal of Petrology 42, 789–823.

Spear, F.S., Kohn, M.J., 1996. Trace element zoning in garnet as a monitor of crustal melting. Geology 24, 1099–1102.
Stevens, G., Clemens, J.D., 1993. Fluid-absent melting and the roles of fluids in the lithosphere: a slanted summary? Chemical Geology 108, 1–17.
Stevens, G., Villaros, A., Moyen, J.-F., 2007. Selective peritectic garnet entrainment as the origin of geochemical diversity in S-type granites. Geology 35, 9–12.
Stöckhert, B., Duyster, J., Trepmann, C., Massonne, H.-J., 2001. Microdiamonds daughter crystals precipitated from supercritical COH + silicate fluids included in garnet, Erzgebirge, Germany. Geology 29, 391–394.
Stüwe, K., 1995. Thermal buffering effects at the solidus. Implications for the equilibration of partially melted metamorphic rocks. Tetonophysics 248, 39–51.
Stüwe, K., 1997. Effective bulk composition changes due to cooling: a model predicting complexities in retrograde reaction textures. Contributions to Mineralogy and Petrology 129, 43–52.
Tuttle, O.F., Bowen, N.L., 1958. Origin of granite in the light of experimental studies in the system: $NaAlSi_3O_8$–$KAlSi_3O_8$–SiO_2–H_2O. Geological Society of America Memoirs 74 (153 pp.).
Van Orman, J.A., Grove, T.L., Shimizu, N., Layne, G.D., 2002. Rare earth element diffusion in a natural pyrope single crystal at 2.8 GPa. Contributions to Mineralogy and Petrology 142, 416–424.
Vielzeuf, D., Holloway, J.R., 1988. Experimental determination of the fluid-absent melting relations in the pelitic system. Contributions to Mineralogy and Petrology 98, 257–276.
Vielzeuf, D., Baronnet, A., Perchuk, A.L., Laporte, D., Baker, M.R., 2007. Calcium diffusivity in alumino-silicate garnets: and experimental and ATEM study. Contributions to Mineralogy and Petrology 154, 153–170.
Villaros, A., Stevens, G., Moyen, J.-F., Buick, I.S., 2009a. The trace element compositions of S-type granites: evidence for disequilibrium melting and accessory phase entrainment in the source. Contributions to Mineralogy and Petrology 158, 543–561.
Villaros, A., Stevens, G., Buick, I.S., 2009b. Tracking S-type granite from source to emplacement: clues from garnet in the Cape Granite Suite. Lithos 112, 217–235.
Wall, V.J., Clemens, J.D., Clarke, D.B., 1987. Models for granitoid evolution and source composition. Journal of Geology 95, 731–749.
Watson, E.B., 1982. Basalt contamination by continental crust: some experiments and models. Contributions to Mineralogy and Petrology 80, 73–87.
Watson, E.B., 1996. Dissolution, growth and survival of zircons during crustal fusion: kinetics principles, geological models and implications for isotopic inheritance. Transactions of the Royal Society of Edinburgh: Earth Sciences 87, 43–56.
Watson, E.B., Baker, D.R., 1991. Chemical diffusion in magmas: an overview of experimental results and geochemical applications. In: Perchuk, L.L., Kushiro, I. (Eds.), Physical Chemistry of Magmas. Springer, Berlin Heidelberg New York, pp. 120–151.
Watt, G.R., Harley, S.L., 1993. Accessory phase controls on the geochemistry of crustal melts and restites produced during water-undersaturated partial melting. Contributions to Mineralogy and Petrology 114, 550–566.
Watt, G.R., Burns, I.M., Graham, G.A., 1996. Chemical characteristics of migmatites: accessory phase distribution and evidence for fast melt segregation rates. Contributions to Mineralogy and Petrology 125, 100–111.
Weinberg, R.F., Hasalová, P., 2015. Water-fluxed melting of the continental crust: a review. Lithos 212–215, 158–188.
White, R.W., Powell, D.R., 2010. Retrograde melt-residue interaction and the formation of near-anhydrous leucosomes in migmatites. Journal of Metamorphic Geology 28, 579–597.
White, R.W., Powell, R., Holland, T.J.B., 2007. Progress relating to calculation of partial melting equilibria for metapelites. Journal of Metamorphic Geology 25, 511–527.
White, R.W., Stevens, G., Johnson, T.E., 2011. Is the crucible reproducible? Reconciling melting experiments with thermodynamic calculations. Elements 7, 241–246.
Zeck, H.P., 1992. Restite-melt and mafic-felsic magma mingling in an S-type dacite, Cerro del Hoyazo, southeastern Spain. Transactions of the Royal Society of Edinburgh: Earth Sciences 83, 139–144.
Zeck, H.P., Williams, I., 2002. Inherited and magmatic zircon from Neogene Hoyazo cordierite dacite, SE Spain-Anatectic source rock provenance and magmatic evolution. Journal of Petrology 43, 1089–1104.
Zhang, Y., Walker, D., Lesher, C.E., 1989. Diffusive crystal dissolution. Contributions to Mineralogy and Petrology 102, 492–513.
Zhang, Y., Ni, H., Chen, Y., 2010. Diffusion data in silicate melts. In: Zhang, Y., Cherniak, D.J. (Eds.), Diffusion in Minerals and Melts. Reviews in Mineralogy and Geochemistry vol. 72, pp. 311–408.